catalysts

MDPI

Review

Carboxylation of Hydroxyaromatic Compounds with HCO_3^- by Enzyme Catalysis: Recent Advances Open the Perspective for Valorization of Lignin-Derived Aromatics

Immacolata C. Tommasi

Dipartimento di Chimica, Università di Bari "A. Moro", v. Orabona, 4, 70126 Bari, Italy; immacolata.tommasi@uniba.it; Tel.: +39-080-5443563

Received: 18 November 2018; Accepted: 22 December 2018; Published: 3 January 2019

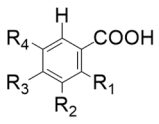


Abstract: This review focuses on recent advances in the field of enzymatic carboxylation reactions of hydroxyaromatic compounds using HCO_3^- (as a CO_2 source) to produce hydroxybenzoic and other phenolic acids in mild conditions with high selectivity and moderate to excellent yield. Nature offers an extensive portfolio of enzymes catalysing reversible decarboxylation of hydroxyaromatic acids, whose equilibrium can be pushed towards the side of the carboxylated products. Extensive structural and mutagenesis studies have allowed recent advances in the understanding of the reaction mechanism of decarboxylase enzymes, ultimately enabling an improved yield and expansion of the scope of the reaction. The topic is of particular relevance today as the scope of the carboxylation reactions can be extended to include lignin-related compounds in view of developing lignin biorefinery technology.

Keywords: carbon dioxide; HCO_3^-; carboxylation reaction; synthesis of hydroxyl aromatic carboxylic acids; enzymatic carboxylation reactions

1. Introduction

Phenolic acids, encompassing both hydroxybenzoic and hydroxycinnamic acids (Figure 1), are important intermediates in the pharmaceutical and agrochemical industry, [1–4] as well as in the synthesis of advanced materials [5–7].



$R_1 = R_2 = R_3 = R_4 = H$; benzoic acid

$R_1 = R_2 = R_4 = H$; $R_3 = OH$; *para*-hydroxybenzoic acid

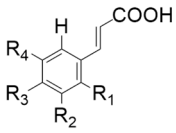
$R_1 = R_4 = H$; $R_2 = OCH_3$; $R_3 = OH$; vanillic acid

$R_1 = R_4 = H$; $R_2 = R_3 = OH$; protocatechuic acid

$R_1 = H$; $R_2 = R_4 = OCH_3$; $R_3 = OH$; syringic acid

$R_1 = R_4 = OH$; $R_2 = R_3 = H$; gentisic acid

$R_1 = OH$; $R_2 = R_3 = R_4 = H$; salicylic acid



$R_1 = R_2 = R_3 = R_4 = H$; cinnamic acid

$R_1 = R_2 = R_4 = H$; $R_3 = OH$; *para*-coumaric acid

$R_1 = R_4 = H$; $R_2 = OCH_3$; $R_3 = OH$; ferulic acid

$R_1 = H$; $R_2 = R4 = OCH_3$; $R_3 = OH$; sinaptic acid

$R_1 = R_4 = H$; $R_2 = R_3 = OH$; caffeic acid

Figure 1. Phenolic acids: Examples of hydroxybenzoic and hydroxycinnamic acids.

From a synthetic point of view, the preparation of hydroxyl-substituted aromatic carboxylic acids by functionalisation of aromatic hydroxy compounds with CO_2 is a highly desirable green procedure alternative to traditional and high temperature oxidation processes using HNO_3 or molecular oxygen [8].

Hydroxybenzoic acids are currently manufactured by the Kolbe Schmitt process, proceeding through an electrophilic aromatic substitution of phenoxide anion with CO_2 [9]. Recently, Larrosa has reported a convenient synthetic method based on the *ortho*-carboxylation of phenols with CO_2, making use of NaH to produce anhydrous phenoxide anions [10].

An attractive alternative synthetic approach to obtain hydroxybenzoic and hydroxycinnamic acids is the use of environmentally friendly enzymatic catalysis. A number of enzymes catalyzing regioselective *ortho*- or *para*-carboxylation of aromatic hydroxy compounds with HCO_3^- have been reported in the literature. Besides, phenolic acid decarboxylases catalyzing carboxylation of *para*-hydroxy styrene derivatives have been recently discovered. Significant advances in bio-carboxylation technology can be expected in the future, thanks to the discovery of new enzymes and recent improvements in synthetic biology techniques [11–15].

In fact, using a synthetic biology technology approach makes possible: i) The development of engineered enzymes with a better "catalytic performance" compared with native enzymes; ii) the development of artificial enzymes able to catalyze specific reactions on new substrates or completely new functionalisation reactions on a given set of chemicals; iii) the overexpression of selected enzymes in a host microorganism (usually *E. coli*) or rewiring of the entire microbial metabolic network to drive the synthesis of targeted products; and iv) the development of completely new "chimeric pathways" by assembling enzymes from different organisms for next generation reaction platforms.

Considering all the above, the aim of this review is to provide an overview of recent advances in enzymatic carboxylation reactions of hydroxyaromatic compounds using HCO_3^-. The literature survey will encompass studies concerning the synthetic scope of carboxylase enzymes as well as their structural and kinetic properties, pointed at elucidating the reaction mechanism.

In recent years, a number of reports concerning the enzymatic carboxylation of hydroxyaromatic compounds derived from lignin breakdown have appeared. Section 2 will focus on the problem of lignin depolymerization and the role of biological valorization of phenolic lignin-derived compounds.

2. Biotechnological Exploitation of Lignin from Biorefineries

Plants are the main producers of hydroxyaromatic compounds as lignin represents around 20–35% of the mass collected from lignocellulosic biomass [16]. Lignin monomer precursors (manly *para*-coumaryl alcohol, coniferyl alcohol, and sinapyl alcohol, Figure 2) [17] play a structural function as monolignols are oxidatively polymerized by plants to phenylpropanoid polymers. Several additional monomers, such as hydroxycinnamic acid [18] and caffeyl alcohol [19], have been found in high amounts in grasses and seed coats, respectively.

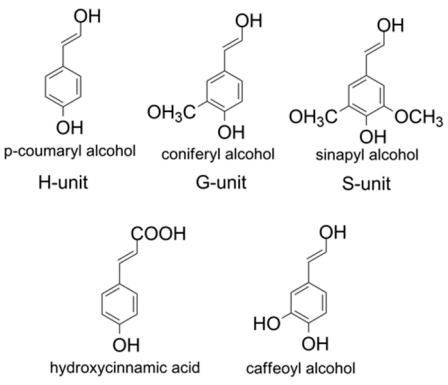


Figure 2. Main lignin monomer precursors produced by plants.

Due to its chemical structure, lignin could serve as a renewable source of aromatic compounds. However, lignocellulosic biorefinery plants commissioned up to date produce pulp, bio-based chemicals, biofuels, electricity, and heat, essentially exploiting the hemicelluloses/cellulose wood fraction and divert the lignin stream to combustion [20]. It is estimated that lignin obtained as a byproduct of the pulp and paper industry is produced at about 50 million tonnes per year globally [21,22]. Therefore, research focused on exploiting this carbon resource is gaining great attention. Actually, valorization of the lignin fraction is hampered by biomass pretreatment and deconstruction strategies, usually affording a material with complex physical properties [20]. Future implementation of lignin biorefinery will require development of new technological approaches for viable conversion of lignin into valuable chemicals.

Targeting aromatic acids (or, more specifically, hydroxyaromatic acids) as chemicals potentially obtainable from lignin biorefinery, a DOE Report published in 2007 (U.S. Department of Energy Report) [23] identifies these chemicals as "high market volume" and "high utility as building blocks", but, at the same time, estimates a "high expected difficulty" to obtain those chemicals from lignin.

It is worth mentioning that, on the laboratory scale, diverse chemical and physicochemical depolymerization processes converting industrially streamed lignin into low molecular mass aromatics have been recently reported. Table 1 reports a non-exhaustive list of such works affording essentially monomeric or oligomeric phenols and phenolic acids.

Table 1. Examples of chemical and physicochemical depolymerization processes converting lignin produced at an industrial level into low molecular mass aromatics.

Technology	Products Obtained	Reference
Thermochemical Process (Fast Pyrolysis)		
The Energy Research Center of the Netherlands (ECN) developed at the laboratory-scale a plant for pyrolysis of technical lignin followed by hydrodeoxygenation using a ruthenium-based catalyst.	Product: Pyrolitic lignin oil (PLO) containing 13–20 wt.% of phenolic fraction consisting of both monomeric and oligomeric phenols. Low molecular weight phenolic compounds was approx. 7–9 wt.%.	[22]
Depolymerization of Organosolv Lignin		
Oxidative depolymerization of lignin in ionic liquids (1-ethyl-3-methylimidazolium trifluoromethanesulfonate in the presence of $Mn(NO_3)_2$ catalyst. (11.2 g of lignin, 111.1 g of IL, 2.22 g of catalyst, treated at 100 °C with air during 24 h).	Product: 66% of lignin conversion (as % weight of initial lignin); 32.7 wt.% of monomeric products extracted from converted lignin (as % weight of initial lignin).	[21]
Organosolv hardwood and wheat straw lignin depolymerized in supercritical carbon dioxide/acetone/water fluid (300-370 °C, 100 bar, during 3.5 h).	Product: Lignin oligomers produced in 18.6% yield (as % weight of dry lignin).	[24]
Chinese fir (softwood) treated by catalytic solvolysis in supercritical alcohol (supercritical ethanol/1-butanol at 300 °C with Ru/C).	Product (when treating Chinese fir lignin): 32.4% of guaiacol-type products 2.34% of syringol-type products (as % selectivity of products detected by GC/MS analysis).	[25]
Non-oxidative depolymerization of *Miscanthus giganteus*-derived lignin in the presence of CH_3CN/THF (10:1) or EtOAc/THF (8:1), 10 wt.% of Vanadium catalyst, at 80 °C, during 24 h.	Product: Approx. 3% of monophenolic compounds (as % weight of treated lignin).	[26]

Analysis of data reported in Table 1 allows one to conclude that a wood pretreatment process with subsequent lignin liquefaction providing monomeric phenolic compounds in high yield and high selectivity is highly desirable.

Beckmann and coworkers [27] have pointed recently that future perspectives to tackle this problem will probably rely on: i) Advances in genetic engineering that have shown that plants carrying mutations in genes coding for lignin biosynthesis pathways and transgenic plants may produce "ideal lignin", allowing improved biopolymer utilization (Figure 3b,c); and ii) valorization of lignin-derived aromatics through new microbiological pathways.

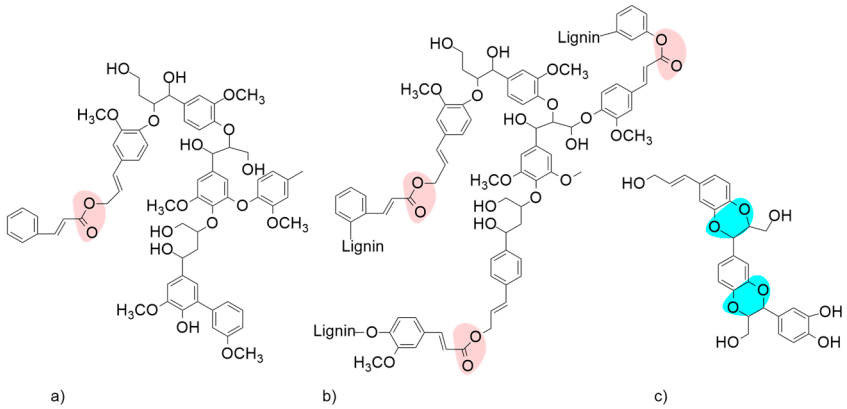


Figure 3. Representation of lignin polymer structures: (**a**) Wild-type lignin; (**b**) engineered lignin with high levels of ferulic acid; (**c**) recently discovered C-lignin. Pink color marks indicate ester linkages. Blue color marks indicate ether linkages. Adapted with permission from [27]. Copyright 2016, Elsevier.

Concerning item i), Wilkerson and coworkers [28] succeeded in engineering poplar trees to produce high level of ferulic acid, increasing the ferulate ester groups into the lignin polymer (Figure 3b). The high degree of ester linkages allowed depolymerisation of the modified lignin under mild alkaline conditions. Moreover, unusual catechyl lignin (C-lignin) (Figure 3c) found in seed coats of *Vanilla planifolia* and various plants of the genus, *Melocactus*, has been converted by hydrogenolysis to produce catechyl-type monomers in a near-quantitative yield with a selectivity of 90% to a single monomer [29].

For item ii), the availability of lignin derived low molecular mass phenolic compounds via efficient depolymerization technologies will provide substrates suitable for microbiological valorization (see Section 11). In fact, microorganisms convert different types of hydroxyaromatic compounds derived from lignin into a few key central intermediates through the so called "channeling" (or "peripheral" or "upper") pathways (Figure 4) [30]. In this way, central intermediates, such as catechol, protocatechuate, and benzoate, are produced in a high yield and selectivity, which is a specific requirement for industrial syntheses.

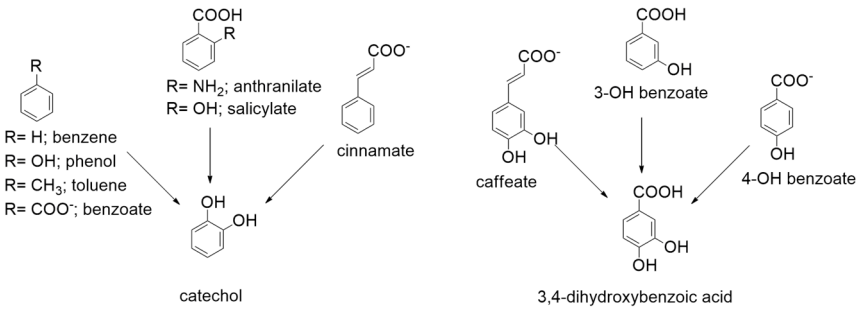


Figure 4. Examples of microbial "channelling aerobic pathways" for the production of aromatic central intermediates [30]. Adapted with permission from [30]. Copyright 2011, Springer Nature.

Central intermediates are further degraded through "central" (or "lower") pathways into intermediary metabolites, such as acetyl-CoA, succinyl-CoA, and pyruvate. Both "channeling" and "lower" pathways have been extensively investigated during the last decades and recently reviewed by Fuchs and coworkers [30].

As relevant examples of biological lignin valorization by aerobic microbial metabolism, it is worth citing: i) The production of *cis*,*cis*-muconate from phenol, guaiacol, or protocachuate by bacteria bearing cytochrome P450 enzymes (Figure 5a). *Cis*,*cis*-muconate can be subsequently converted by chemo-catalysis into terephtalate [31]; and ii) the use of *Pseudomonas putida* KT2440 to convert

protocatechuate into polyhydroxyacid (PHA) (produced at 32% of cell dry weight), as reported by Beckham and coworkers (Figure 5b) [32].

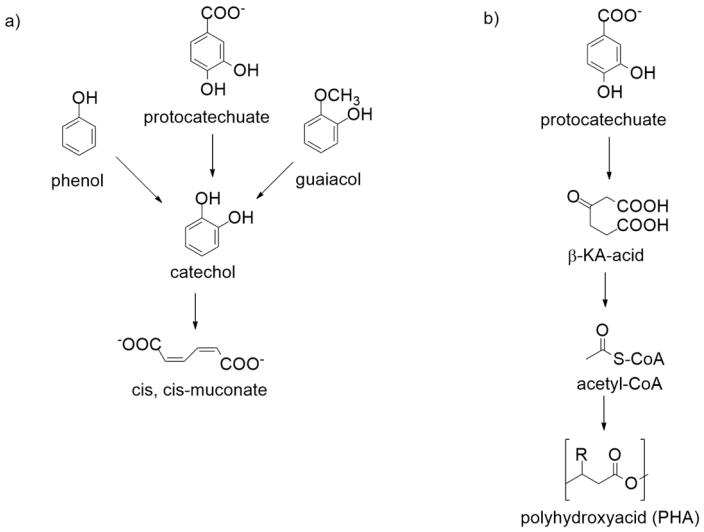


Figure 5. Production of (**a**) *cis*,*cis*-muconate and (**b**) polyhydroxyacid (PHA) by aerobic microbial metabolism. Adapted with permission from [32]. Copyright 2014, National Academy of Science.

Although the abovementioned bio-technological lignin conversion processes use aerobic bacteria metabolism (Figure 5), nature offers a variety of rarely exploited "channeling" and "central" pathways operating in anaerobic microorganisms [33] that reveal unusual reactions as reversible non-oxidative carboxylation of aromatic hydroxy compounds with HCO_3^- to produce *para*-hydroxybenzoic acids (Figure 6) [30,34,35]. As a common microbial strategy, the carboxyl group is converted into thioesters.

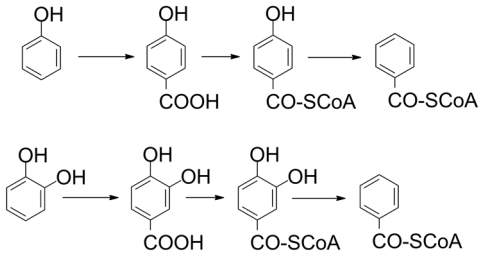


Figure 6. Examples of anaerobic carboxylation reactions of phenol and catechol.

As a note, aromatic hydrocarbons, such as benzene, naphthalene, and toluene, which are mainly produced by human activities, can also be degraded by microorganisms in anaerobic conditions through bio-carboxylation reactions (see Section 10).

From the short analysis reported above, it can be expected that biotechnological technology may contribute significantly to the implementation of lignin biorefinery.

In recent reviews, Chaiyen and coworkers [36] have summarized the most important biotransformations of plant derived phenolic compounds through esterification, decarboxylation, amination, halogenation, and hydroxylation reactions, while Sieber and coworkers have highlighted the importance of several decarboxylase enzymes to produce valuable chemicals from renewable resources [37]. Other relevant reviews dealing with enzymatic carboxylation reactions using CO_2 or HCO_3^- can be found in the literature [38–41]. As mentioned before, in this review, we will focus on the reactivity of decarboxylase enzymes converting hydroxyaromatic compounds into phenolic acids, including recent advances in crystal structure determination and enzyme kinetics.

3. Thermodynamic Considerations

ΔG° values for the carboxylation reaction of several hydroxy aromatic compounds with CO_2 have been calculated to be positive (Figure 7a,b) [42] by using the IEFPCM(H_2O)-G3MP2B3 program. Interestingly, Faber and coworkers have estimated a ΔG° value of 5.2 ± 0.03 kcal/mol (at 30 °C) for the carboxylation of catechol to 2,3-dihydrobenzoate using HCO_3^- (as a CO_2 source) (Figure 8c) catalyzed by 2,6-dihydroxybenzoate decarboxylase [43].

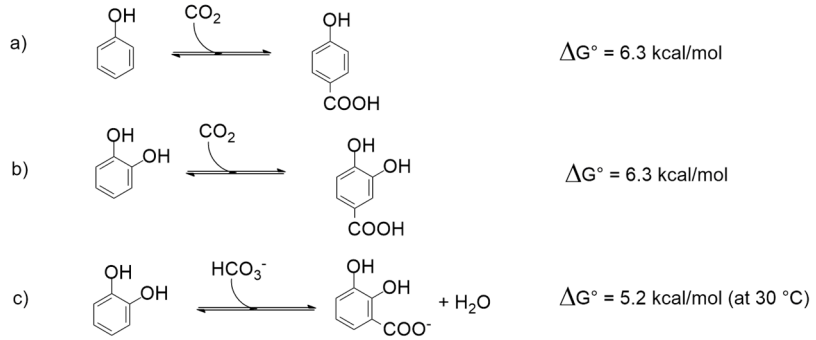


Figure 7. ΔG° for the carboxylation reaction of (**a**) phenol, and (**b**,**c**) catechol as calculated by Faber and coworkers.

Because of thermodynamic constraints, when studying in vitro the carboxylation reaction of phenols or hydroxy styrene derivatives and HCO_3^- to yield benzoate or hydroxycinnamate derivatives, it is necessary to find an appropriate set of experimental conditions to drive forward the uphill carboxylation reaction. Usually, aromatic hydroxy compounds and HCO_3^- are used at elevated concentrations and, in some cases, the carboxylated product is removed from the reaction medium.

Considering that the uphill carboxylation reactions described in this review are always carried out in solutions saturated with $KHCO_3$ (3 M, pH 8.3), the question arises whether CO_2 or HCO_3^- is the real substrate of the reaction. It is possible to determine which of CO_2 or HCO_3^- is the real substrate for the enzyme catalyzed reaction by performing several standard tests reported in the literature [44]. Some reference works published by Faber and coworkers [43,45] consider HCO_3^- as the actual substrate. Moreover, the substrate is often loaded at concentrations that are about two orders of magnitude lower than the saturating $KHCO_3$ concentration.

Based on the abovementioned considerations, it will be assumed that the stoichiometry of the carboxylation reactions analyzed in this review is written according to Figure 7c. The benzoate anion derivatives or hydroxycinnamate derivatives are the reaction products also for carboxylation reactions analysed in Sections 5, 8 and 9. Recovery of the corresponding acid derivative requires subsequent acidification of the reaction medium.

Although the physiological role of decarboxylase enzymes in the microbial anaerobic metabolism may vary, most of the enzymes characterized to date have been named "decarboxylases" as for the thermodynamically favored reaction.

It is worth mentioning that in several enzymes classified as "assimilatory carboxylases" [46], the benzoate derivative is used by microorganisms as a source of carbon and energy. In these cases, the functionalisation of phenols with the carboxyl group increases the molecular polarity and, consequently, increases the water solubility of the carbon source [47].

4. Electron-Rich Heteroaromatic Biocarboxylations

According to Faber classification [45] the enzymatic carboxylation of electron-rich (hetero)aromatics can be divided into four major categories:

1) Decarboxylase enzymes, including salicylic acid decarboxylase, 2,3-dihydroxybenzoate decarboxylase, and 2,6-dihydroxybenzoate decarboxylase, catalysing the regioselective *ortho*-carboxylation of phenols to the directing phenolic group;
2) carboxylase enzymes, including 4-hydrobenzoate and 3,4-dihydroxybenzoate decarboxylases, catalysing the regioselective *para*-carboxylation of phenols to the directing phenolic group. Phenylphosphate carboxylases also belong to this category, but require an adenosine triphosphate (ATP) consuming activation prior to carboxylation;
3) enzymes catalyzing the carboxylation of *para*-hydroxystyrenes at the β-carbon of the styrene side chain, yielding (*E*)-4-hydroxycinnamic acids;
4) enzymes catalyzing carboxylation of heteroaromatics, such as pyrrole and indole, as pyrrole-2-carboxylate and indole-3-carboxylate decarboxylases.

All enzymes mentioned above share the following common features:

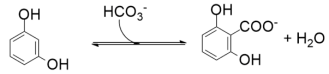
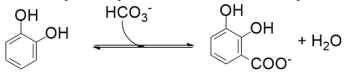
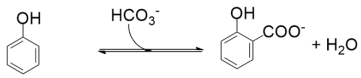
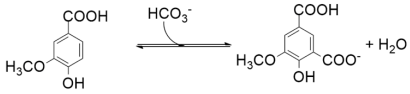
1) Do not need cofactors as pyridoxal 5′-phosphate or thiamine pyrophosphate;
2) substrates are not preactivated by phosphorylation (except for phenylphosphate carboxylase from facultative anaerobes);
3) use of HCO_3^- as a CO_2 source.

Decarboxylase enzymes, classified into categories 1–3, are the subject of this review.

5. Enzymatic Regioselective *Ortho*-Carboxylation of Phenols: The Enzyme's Catalytic Reactivity

The reversible non-oxidative carboxylation of phenols to yield *ortho*-hydroxy benzoate derivatives has been widely investigated in the last decade. A list of characterized decarboxylase enzymes catalyzing the selective *ortho*-carboxylation reaction of hydroxy aromatic compounds is reported in Table 2. For each enzyme, the representative carboxylation reaction is shown, although many of these catalysts convert a broad scope of substrates.

Table 2. List of decarboxylase enzymes catalyzing selective *ortho*-carboxylation reactions recently characterized.

Entry	Enzyme	Microorganism	Reference
1	2,6-dihydroxybenzoic acid decarboxylase (2,6-DHBD) also named γ-resorcylate decarboxylase (γ-RSD) 	*Rhizobium sporomusa* MTP-10005 *Rhizobium radiobacter* WU-0108 *Agrobacterium tumefaciens* IAM12048 *Pandoraea* sp. 12B-2 *Rhodococcus jostii* RHA1 *Polaromonas sporomusa* JS666	[48,49] [50] [51] [52] [53] [54]
2	2,3-dihydroxybenzoate decarboxylase 	*Aspergillus oryzae* *Fusarium oxysporum*	[55] [56]
3	salicylic acid decarboxylase 	*Trichosporon moniliiforme*	[57]
4	5-carboxyvanillate decarboxylase 	*Sphingomonas paucimobilis SYK-6* (LigW_Sp and LigW2_Sp)	[58,59]

5.1. Catalytic Activity of 2,6-Dihydroxybenzoate Decarboxylase from Rhizobium sporomusa, 2,3-Dihydroxybenzoate Decarboxylase from Aspergillus oryzae and Salicylic Acid Decarboxylase from Trichosporon moniliiforme

Faber and coworkers have reported [45] the biocatalytic synthesis of salicylate derivatives starting from substituted phenols (as alkyl-, alkoxy-, halo-, and amino-substituted phenols) and HCO_3^- by using

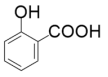
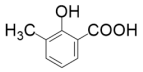
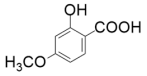
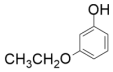
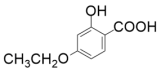
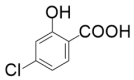
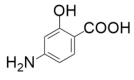
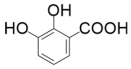
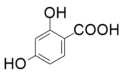
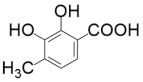
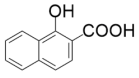
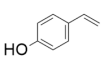
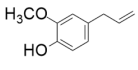
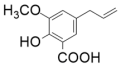
2,6-dihydroxybenzoate decarboxylase from *Rhizobium sporomusa* (2,6-DHBD_Rs), 2,3-dihydroxybenzoate decarboxylase from *Aspergillus oryzae* (2,3-DHBD_Ao), and salicylic acid decarboxylase from *Trichosporon moniliiforme* (SAD_Tm) (the general reaction is shown in Table 2, entries 1–3).

The enzymes were synthesized, subcloned in a pET vector, and overexpressed in a standard *E. coli* BL21(DE3) host, which was transformed with the particular plasmide using standard techniques.

Both thermodynamically favored decarboxylation and thermodynamically disfavored bio-carboxylation reactions were studied.

Carboxylation tests were performed in vitro by using 30 mg of lyophilized cells containing the over-expressed enzymes suspended in phosphate buffer (pH = 8.5, 100 mM), loaded with phenols (10 mM) and $KHCO_3$ (3 M), and incubated at 30 °C during 24 h. All tested substrates underwent highly selective *ortho*-carboxylation with respect to the -OH directing group, with conversion typically ranging from 20% to 80% (Table 3) [60]. Resorcinol (entries 8 and 9) afforded two carboxylate products.

Table 3. Selective *ortho*-carboxylation of mono- and di-substituted phenols using HCO_3^- (selected examples from Ref. 45). Adapted with permission from [45]. Copyright 2014, Royal Society of Chemistry.

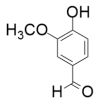
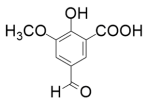
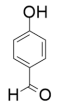
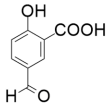
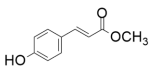
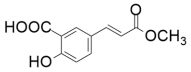
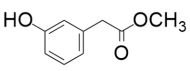
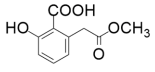
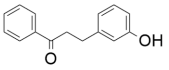
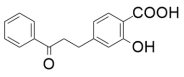
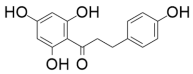
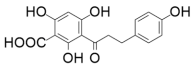
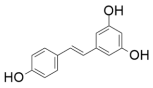
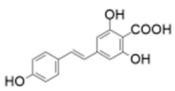
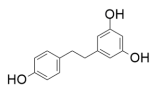
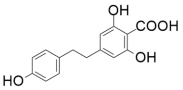
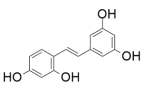
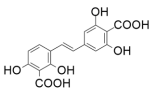
Entry	Substrate	Product	2,3-DHBD_Ao Conversion (%)	SAD_Tm Conversion (%)	2,6-DHBD_Rs Conversion (%)
1			43	43	<1
2			16	30	<1
3			50	48	12
4			48	47	18
5			25	22	1
6			74	80	5
7			30	21	35
8			22	30	31
9			29	40	<1
10			15	28	37
11			54	62	46
12			58	29	<1
13			14	5	<1

2,6-DHBD_Rs showed a more restricted substrate scope with respect to 2,3-DHBD_Ao and SAD_Tm. The electronic nature of the substituent did not influence significantly the yield of the carboxylated product unless strong electron-withdrawing substituents as -NO_2 or -CO were present (not shown in Table 3). Alkyl-, alkoxy-, halo-, and amino-phenols substituted at the *meta*-position yielded a higher conversion with respect to corresponding *ortho*- and *para*-substituted analogs (not shown in Table 3).

It is worth noting that the tuberculostatic agent, *para*-aminosalicylic acid (entry 6), was obtained in 80% conversion by the enzymatic reactions. The product can be also obtained in 80% yield by the Kolbe-Schmitt process, although at a considerably higher temperature and pressure (90 bar, 120–130 °C).

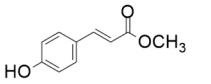
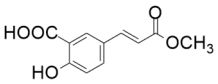
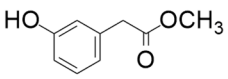
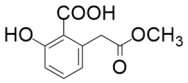
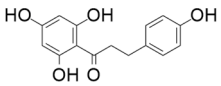
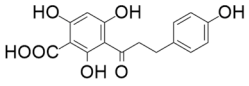
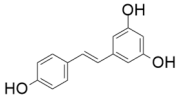
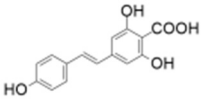
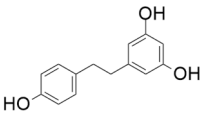
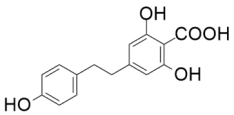
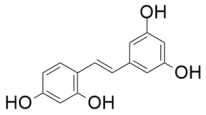
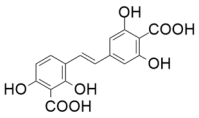
Very recently, Faber and coworkers [61] have used the same set of decarboxylase enzymes (i.e., 2,6-dihydroxybenzoate decarboxylase from *Rhizobium sporomusa*, 2,3-dihydroxybenzoate decarboxylase from *Aspergillus oryzae*, and salicylic acid decarboxylase from *Trichosporon moniliiforme*) overexpressed in *E. coli* to test the regioselective carboxylation of several phenols (entries 1–5) and bioactive polyphenols (Table 4). Polyphenols are well known for their biological activities as antioxidants, anti-inflammatory, and antimicrobial agents [62]. Faber argues that the newly introduced carboxylate-functionalisation in the aromatic ring should improve the stability of the molecule and that the obtained phenolic acids are expected to impede light-induced degradation as demonstrated for other photolabile substances, such as vitamins and nucleic acids [63]. The carboxylation reaction was performed under experimental conditions optimized in the previous work [45] (i.e., 30 mg of *E. coli* lyophilized cells/mL, phosphate buffer (pH 8.5, 100 mM), substrate (10 mM), $KHCO_3$ (3 M), at 30 °C, during 24 h).

Table 4. Carboxylation of phenols and polyphenols by 2,3-DHBD_Ao, 2,6-DHBD_Rs and SAD_Tm enzymes. Adapted with permission from [61]. Copyright 2017, John Wiley and Sons.

Entry	Substrate	Product	2,3-DHBD_Ao Conversion (%)	2,6-DHBD_Rs Conversion (%)	SAD_Tm Conversion (%)
1			40	<1	33
2			62	<1	<1
3			33	<1	32
4			66	<1	<1
5			68	57	68
6			97	97	60
7			85	97	96
8			65	77	45
9			83	97	96

It is of note that polyphenols (entries 6–9) yielded better results, affording carboxylate products with conversions ranging from 60 to 97%. For the most promising substrates, the reactions were performed on a preparative scale using the following experimental conditions: 651 mg of *E. coli* lyophilized cells suspended in 19 mL of phosphate buffer (pH 8.5, 100 mM) containing the substrate (10–11 mM) and $KHCO_3$ (3 M). Methanol was also used as a water-miscible organic co-solvent. Cells were incubated at 30 °C during 24 h. As shown in Table 5, carboxylate products were obtained in moderate to excellent yields.

Table 5. Carboxylation of phenols and polyphenols under preparative conditions. Adapted with permission from [61]. Copyright 2017, John Wiley and Sons.

Entry	Substrate	Product	2,3-DHBD_Ao Yield (%)	2,6-DHBD_Rs Yield (%)
3			32	-
4			43	-
6			67	-
7			-	95
8			-	45
10			-	66

Very recently, Glueck, Faber, and coworkers succeeded in optimizing the reaction conditions, allowing one to carry out the carboxylation reaction of resorcinol under CO_2 pressure (30–40 bar) instead of using HCO_3^-. The carboxylated products were obtained in a 68% yield and 100% atom economy [64]. 2,3-DHBD_Ao and 2,6-DHBD_Rs were tested under the new reaction conditions. 2,3-DHBD_Ao actively catalyzed the carboxylation reaction while 2,6-DHBD_Rs underwent irreversible inactivation under CO_2-pressure.

The optimized reaction conditions were as follows: Lyophilized whole cells (90 mg) of *E. coli* host cells containing the overexpressed enzymes were rehydrated in Tris-HCl buffer (pH 9.0, 100 mM), loaded with the substrate (10 mM), and subsequently transferred into a high pressure reactor. After CO_2 gas was applied (30–40 bar), the reaction mixture was stirred for 24 h at 30 °C.

Following the seminal studies reported above, a recent publication from Zhu and coworkers [65] reported the high yield carboxylation of resorcinol and catechol to 2,6-dihydroxybenzoate and 2,3-dihydroxybenzoate, respectively (representative reactions are shown in Table 2, entries 1 and 2) by using 2,6-dihydroxybenzoate decarboxylase from *Rhizobium sporomusa* in the presence of a quaternary ammonium salt added to the reaction system.

Knowing from the literature that tetrabutylammonium chloride forms an insoluble salt with 2,6-dihydroxybenzoate in alkaline solutions, the formation of water-insoluble salts was exploited to drive the carboxylation equilibrium toward the side of the carboxylate product. *E. coli* cells overexpressing the enzyme (16 mg) were suspended in a saturated $KHCO_3$ solution, and loaded with the substrate (resorcinol or catechol, 10 mM) and the quaternary ammonium salt, which was added at the concentration of 20 mM or 50 mM. Incubation was carried out at 30 °C during 24 h for resorcinol and during 48 h for catechol.

To find the salt that was better performed as the precipitating reagent, an array of nine quaternary ammonium halide salts were tested in resorcinol carboxylation. Better results were obtained by using tetrabutylammonium bromide at 50 mM (2,6-dihydroxybenzoate was obtained in a 97% yield). To upscale the reaction, 400 mg of *E. coli* cells were charged with resorcinol (200 mM) and tetrabutylammonium bromide (250 mM) to yield 99% of 2,6-dihydroxybenzoate after 48 h of reaction (as determined by HPLC analysis). After treatment with hydrochloric acid, the benzoate-ammonium salt and the benzoic acid derivative was isolated in a 72% yield and the quaternary ammonium salt could be extracted and recycled.

By using catechol as a substrate, better results were obtained with the addition of dodecyldimethylbenzylammonium chloride and tetradecyldimethylbenzyl ammonium chloride at the concentration of 20 mM, which afforded the 2,3-dihydroxybenzoate salt in a 97% and 95% yield, respectively.

5.2. Catalytic Activity of 2,3-Dihydroxybenzoic Acid Decarboxylase from Fusarium oxysporum (2,3-DHBD_Fo)

The research group of Zhou [66] succeeded recently in isolating a new enzyme, 2,3-dihydroxybenzoic acid decarboxylase from *Fusarium oxysporum*, thus expanding the toolbox for phenols' carboxylation (the representative reaction is shown in Table 2, entry 2). The enzyme shows a molecular mass of 143.6 kDa, suggesting a homotetrameric structure similar to 2,3-DHBD_Ao, 2,6-DHBD_Rs, and SAD_Tm proteins. The sequence alignment comparison with 2,6-DHBD_Rs showed a 45% amino acid identity. Amino acids of the catalytic triad found in 2,6-DHBD_Rs (Asp287, His218, Glu221, see Section 6.1) are conserved in 2,3-DHBD_Fo.

2,3-DHBD_Fo shows a surprisingly high substrate tolerance as the highest enzymatic reaction rate can be measured at the substrate concentration of 200 mM. In comparison, for 2,6-DHBD_Rs, the highest reaction rate can be measured for a resorcinol concentration of 45 mM and for SAD_Tm, the highest reaction rate can be measured for a phenol concentration of 30 mM.

Zhu and coworkers have measured a K_M of 24.9 ± 4.13 mM and k_{cat} of 46.8 ± 0.01 min^{-1} for the purified enzyme catalyzing the carboxylation of catechol to 2,3-dihydroxybenzoate. Table 6 shows the scope of the carboxylation reaction carried out by using the purified enzyme under the following experimental conditions: 96 μg of protein was suspended in 1 mL containing 20 mM of substrate and 3 M of $KHCO_3$. Cells were incubated at 40 °C for 20 min.

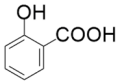
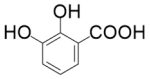
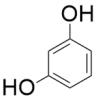
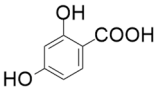
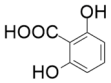
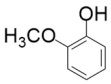
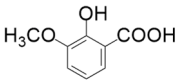
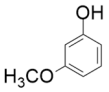
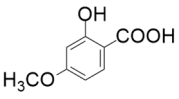
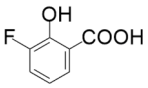
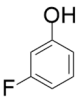
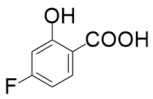
As can be seen in entries 3 and 4 of Table 6, resorcinol carboxylation may afford two products. A greater conversion in catechol carboxylation (95% within 3h) was obtained by using *E. coli* whole cells overexpressing the enzyme in conjunction with dodecyldimethylbenzylammonium chloride salt.

In view of industrial applications, Kara and coworkers [67] suggested the use of CO_2 in the carboxylation reactions instead of $KHCO_3$. In situ formation of the $[HCO_3^-][^+HNR_3]$ salt was favored in the presence of tertiary amines under a CO_2 atmosphere.

E. coli cells overexpressing 2,3-dihydroxybenzoate decarboxylase from *Aspergillum oryzae* (3 mg/mL corresponding to 0.23 U/mL) were suspended in screw-capped glass vials (1.5 mL) containing a buffer solution (potassium phosphate 0.1 M, pH = 7.5) with addition of triethylamine (1 M), catechol (10 mM), and ascorbic acid (10 mM) under CO_2 constant bubbling at ambient pressure and at 30 °C. The maximal conversion of catechol in the reported conditions was 25%, which was

higher when compared with the 14% conversion obtained in the presence of $KHCO_3$ 1 M. The use of secondary and primary amines resulted in lower yields.

Table 6. Scope of the carboxylation reaction catalyzed by 2,3-DHBD_Fo (purified protein). Adapted with permission from [66]. Copyright 2018, Elsevier.

Entry	Substrate	Product	2,3-DHBD_Fo Conversion (%)
1			33
2			28
3			9
4			35
5			15
6			46
7			4.8
8			7.8

The authors ascribe the increase in substrate conversion to the interaction between alkylammonium ions [HNR_3^+] and catechol in the active site of the enzyme. It is important to note that the results reported by Zhu and coworkers (see Section 5.1) were obtained in the presence of sterically hindered ammonium quaternary salts.

5.3. Catalytic Activity of Mutated Salicylic Acid Decarboxylase from Trichosporon moniliiforme

The research group of Kirimura [68] has identified and subsequently characterized a salicylic acid decarboxylase from *Trichosporon moniliiforme* WU-0401 yeast, catalyzing the reversible and regioselective carboxylation of phenol to salicylate with HCO_3^- (the representative reaction is shown in Table 2, entry 3). Later, the authors succeeded in obtaining a F195Y-salicylic acid decarboxylase mutant showing a higher specificity toward carboxylation of *meta*-aminophenol to *para*-aminosalicylate, an antituberculosis agent [69] (Figure 8).

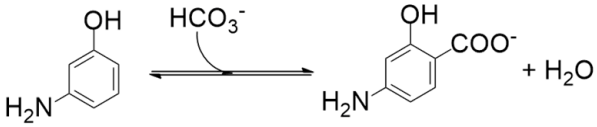


Figure 8. Reversible carboxylation reactions catalyzed by salicylic acid decarboxylase enzyme from *Trichosporon moniliiforme* WU-0401 yeast.

The F195Y-salicylic acid decarboxylase mutant was overexpressed in *E. coli* BL21(DE3) and the recombinant whole cells were used for *para*-aminosalicylate production from *meta*-aminophenol.

More recently [70], Kirimura and coworkers were able to generate a Y64T-F195Y-salicylic acid decarboxylase mutant, which exhibited a superior catalytic activity toward selective *meta*-aminophenol carboxylation to *para*-aminosalicylate when compared with the wild-type enzyme. In particular, the double mutant salicylic acid decarboxylase showed excellent substrate tolerance (200 mM substrate concentrations, which was two times higher than the substrate concentration tolerated by the wild-type protein), producing *para*-aminosalicylate at 140 mM (corresponding to a substrate conversion of 70%). Essays were performed by using whole-cell recombinant *E. coli* BL21(DE3) suspended in a phosphate buffer at pH 6.0, contacted with 2 M $KHCO_3$, and incubated within 9 h, at 30 °C.

Table 7 compares the substrate conversion obtained by using 2,6-DHBD_Rs, 2,3-DHBD_Ao and 2,3-DHBD_Fo enzymes in the *ortho*-carboxylation reaction of catechol and resorcinol. Under typical experimental conditions, a conversion ranging from 20% to 35% is obtained. Conversion could be significantly improved up to 68% under CO_2 pressure (30–40 bar) or up to 97% by addition of the quaternary ammonium salts.

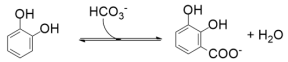
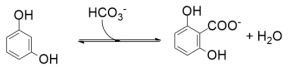
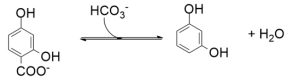
5.4. Bio-Catalysis of 5-Carboxyvanillate Decarboxylase Enzymes from Sphingomonas paucimobilis SYK-6 (LigW_Sp and LigW2_Sp)

5-carboxyvanillate decarboxylases from *Sphingomonas paucimobilis SYK-6* (LigW_Sp and LigW2_Sp) have been recently characterized as enzymes playing a role in lignin degradation through the 5-carboxyvanillate pathway [71,72] and as proteins catalysing the reversible carboxylation of vanillate to 5-carboxyvanillate (the representative reaction shown in Table 2, entry 4) [56,57]. Very recently, Zhao and coworkers [73] have used LigW_Sp and LigW2_Sp enzymes in carboxylation reactions of various lignin derived phenols (Table 8).

Lyophilized *E. coli* whole cells (30 mg) containing overexpressed decarboxylases, LigW_Sp, LigW2_Sp, and 2,3-DHBD_Ao, were incubated with selected substrates (at the concentration of 10 mM) in 1 mL of phosphate buffer (100 mM, pH 8.5) in the presence of 3 M $KHCO_3$ at 30 °C, during 24 h.

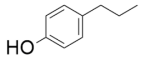
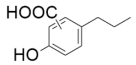
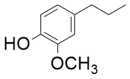
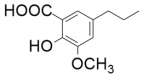
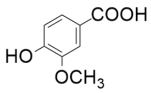
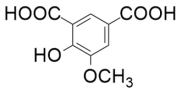
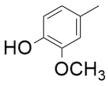
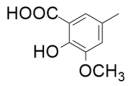
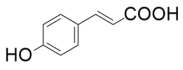
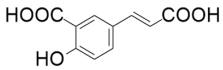
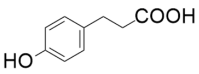
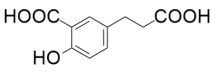
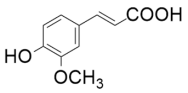
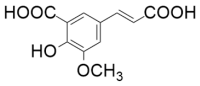
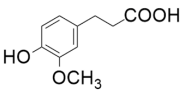
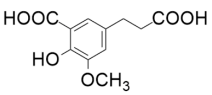
The authors highlight the importance of products listed in Table 8, noting that most of these carboxylates can be used as monomers in polyesters synthesis. In particular, the caffeic acid analogue shown in entry 5 exhibits a significant antioxidant activity in primary cortical neuron cells and can be synthesized by a conventional method in a multistep process with a 10.2% overall yield.

Table 7. Comparison of substrate conversion obtained by using 2,6-DHBD_Rs, 2,3-DHBD_Ao, 2,3-DHBD_Fo, and SAD_Tm enzymes in *ortho*-carboxylation reactions of catechol and resorcinol.

	2,3-DHBD_Ao (a) Conversion %	2,6-DHBD_Rs (a) Conversion%	2,3-DHBD_Ao (b) Conversion %	2,6-DHBD_Rs (c) Conversion %	2,3-DHBD_Ao (d) Conversion %	2,3-DHBD_Fo (e) Conversion %	2,3-DHBD_Fo (f) Conversion %
	30	35	-	97	25	28	95
	22	31	68	97	-	35	-
	29	<1	-	0.1	-	9	-

(**a**): 30 mg of lyophilized cells containing the overexpressed enzymes (2,6-DHBD_Rs, 2,3-DHBD_Ao) were suspended in a phosphate buffer (pH = 8.5, 100 mM), loaded with phenols (10 mM) and $KHCO_3$ (3 M), and incubated at 30 °C during 24 h. (**b**) Lyophilized whole cells (90 mg) of *E. coli* host cells containing the 2,3-DHBD_Ao overexpressed enzyme were rehydrated in TRIS-HCl buffer (pH 9.0, 100 mM), loaded with the substrate (10 mM), and subsequently transferred into a pressure reactor. After closing the reactor, CO_2 gas was applied (30 - 40 bar) and the reaction mixture was stirred for 24 h at 30 °C. (**c**): *E. coli* cells overexpressing the 2,6-DHBD_Rs enzyme (16 mg) were suspended in saturated $KHCO_3$ solution, loaded with the substrate (resorcinol or catechol, 10 mM) and the quaternary ammonium salt (dodecyldimethylbenzylammonium chloride, 20 mM for catechol; tetrabutylammonium bromide, 50 mM for resorcinol). Incubation was carried out at 30 °C during 24 h for resorcinol and during 48 h for catechol. (**d**): *E. coli* cells overexpressing 2,3-dihydroxybenzoate decarboxylase from *Aspergillum oryzae* (3 mg/mL corresponding to 0.23 U/mL) were suspended in screw-capped glass vials (1.5 mL) containing buffer solution (potassium phosphate 0.1 M, pH = 7.5) with addition of triethylamine (1 M), catechol (10 mM), and ascorbic acid (10 mM) under CO_2 constant bubbling at ambient pressure and at 30 °C. (**e**): 96 μg of protein (2,3-DHBD_Fo) were suspended in 1 mL containing 20 mM of substrate and 3 M of $KHCO_3$. Cells were incubated at 40 °C for 20 min. (**f**): *E. coli* whole cells overexpressing 2,3-DHBD_Fo in combination with dodecyldimethylbenzylammonium chloride salt.

Table 8. Phenols and phenolic acids potentially obtainable from lignin depolymerization carboxylated by LigW_Sp, LigW2_Sp, and 2,3-DHBD_Ao enzymes. Adapted with permission from [73]. Copyright 2018, Elsevier.

Entry	Substrate	Product	LigW_Sp Conversion (%)	LigW2_Sp Conversion (%)	2,3-DHBD_Ao Conversion (%)
1			6	1	9.9
2			10.2	7.3	4.2
3			19.4	20.3	<1
4			16.6	13.9	9.3
5			9.0	26.6	7.2
6			5.1	28.0	<1
7			31.3	18.0	25.4
8			18.7	12.4	4.4

6. Insights into the Reaction Mechanism of Decarboxylase Enzymes: Protein Structure

6.1. 2,6-Dihydroxybenzoate Decarboxylase from Rhizobium sporomusa

A reference study on enzymatic *ortho*-carboxylation of phenols has been reported by Goto and coworkers in 2006 [74]. The authors succeeded in solving the crystal structure of 2,6-dihydroxybenzoic acid decarboxylase from *Rhizobium sporomusa* (the representative reaction is shown in Table 2, entry 1) both in its native form and complexed with 2,6-dihydroxybenzoate up to a 1.70 and 1.90 Å resolution, respectively. The overall crystal structure shows a homotetramer, where each subunit bears a Zn^{2+} ion in the catalytic core and one substrate molecule. Each subunit shows a $(\alpha/\beta)_8$-TIM-barrel tertiary fold completed by three linker peptides located at specific positions between β-strands and α-helices and a C-terminal tail. A schematic diagram of the active site of the protein in a complex with 2,6-dihydroxybenzoate is shown in Figure 9A. The structure reveals the Zn^{2+} cation being coordinated by four amino acidic residues (Asp287, Glu8, His10, and His164) and one water molecule (not shown in Figure 9A) in a distorted trigonal bipyramidal geometry.

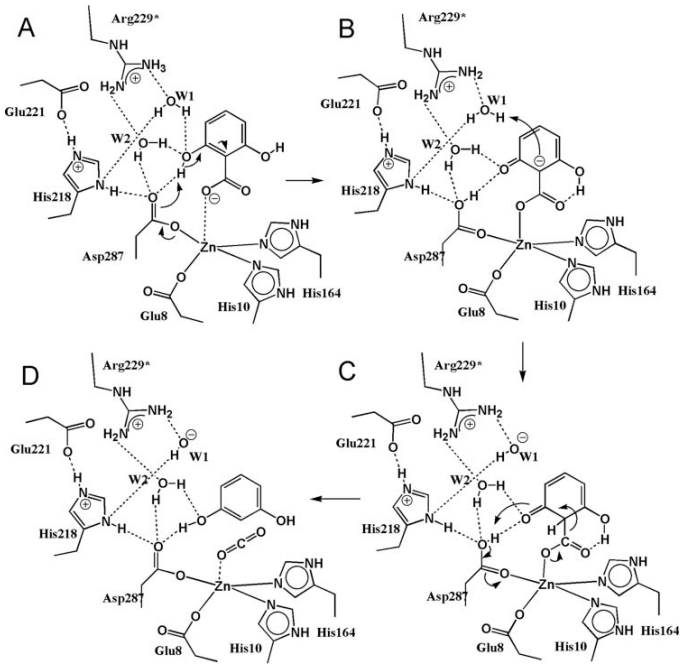


Figure 9. Schematic diagram showing the 2,6-dihydroxybenzoate decarboxylase active site. (**A**) Coordination environment of Zn^{2+} with the 2,6-dihydroxybenzoate ligand; (**B**,**C**,**D**) representation of intermediates formed during the decarboxylation reaction Reproduced with permission from [74]. Copyright 2006, American Society for Biochemistry and Molecular Biology.

Goto proposed a possible reaction mechanism initiated by binding of the substrate to Zn^{2+} in a mono-dentate mode with a distance of 2.0 Å (Figure 10A). By docking the benzoate derivative into the active site and refining the model by energy minimization of the selected binding modes, the authors showed that the C2-hydroxyl group of the benzoate derivative is engaged in hydrogen-bonding with the carboxylate group of Asp287 that, in turn, is part of a catalytic triad together with His218 and Glu221. Moreover, two water molecules (W1 and W2) were shown engaging in hydrogen bonding with Arg229.

The authors suggest the carboxylate group of Asp287 (involved in the catalytic triad) abstracts the proton from the 2-hydroxyl group of the substrate (Figure 9B), allowing the subsequent delocalization of a negative charge at the C1-position of the ring. Protonation at the C1-position of the ring from W1 is followed by re-aromatization, leading to the decarboxylation.

Faber and coworkers have recently reanalyzed the crystal structure of 2,6-dihydroxybenzoate decarboxylase from *Rhizobium sporomusa* (strain MTP-10005) solved by Goto and coworkers, proposing a reaction mechanism for the uphill carboxylation reaction of resorcinol to 2,6-dihydroxybenzoate with HCO_3^- [45]. Faber assumes that the carboxylation reaction is initiated by Asp287 and engaged into hydrogen abstraction from the phenolic hydroxyl group (Figure 10) (Asp287 is in turn activated through the triad with His218 and Glu221), while HCO_3^- is stabilized by coordination to the Zn^{2+} cation. Subsequently, the enhanced nucleophilicity at the C2-position of resorcinolate anion enables a nucleophilic attack onto HCO_3^- with the formation of the oxyanion intermediate shown in Figure 10.

Moreover, three water molecules (W1, W2, and W3, in Figure 10), which are structurally conserved, are triggered by Asn128 via a protonation-deprotonation sequence, enabling H_2O elimination from the oxyanion intermediate and re-aromatization of the ring to afford the Zn^{2+}-carboxylate product. Finally, 2,6-hydroxybenzoate is exchanged at the active site with resorcinol and HCO_3^-.

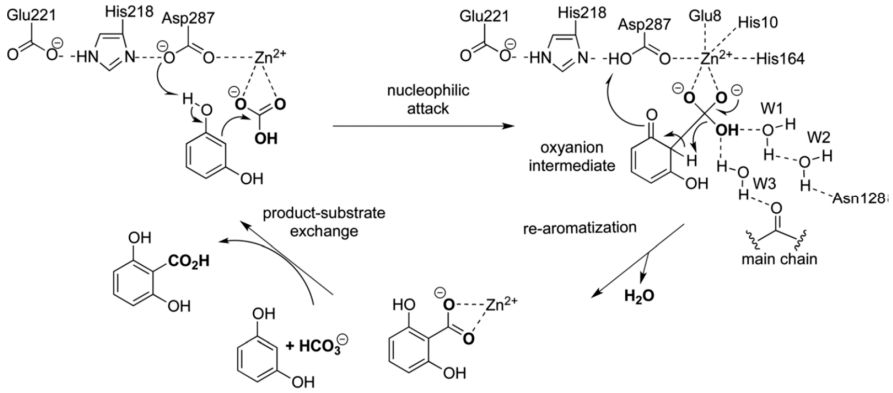


Figure 10. Proposed catalytic mechanism for the *ortho*-carboxylation of resorcinol based on the crystal structure of 2,6-dihydroxybenzoate decarboxylase from *Rhizobium* sp. 38 (Protein Data Bank (PDB)-Code: 2DVU) supported by docking experiments. Adapted with permission from [45]. Copyright 2014, Royal Society of Chemistry.

The above-mentioned mechanism was supported by a molecular docking approach by using the PyMOL Molecular Graphics System to build a 3D molecular model of the active site of the enzyme (Figure 11A) based on the crystal structure obtained by Goto and coworkers. Both 2,6-hydroxybenzoate (Figure 11A) and the proposed oxyanion intermediate (Figure 11B) were docked into the active site and the model was refined by energy minimization of the selected binding modes. The hydrogen bonding network displayed in the 3D model fully supports the proposed reaction mechanism.

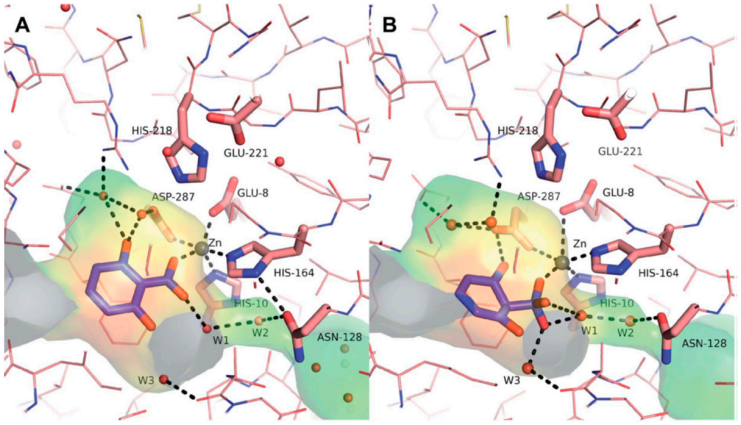


Figure 11. 3D model of the active site of 2,6-DHBD_Rs based on the crystal structure of 2,6-DHBD_Rs (PDB-Code: 2DVU). (**A**): 2,6-dihydroxybenzoate docked into active site; (**B**): Energy minimized docking of the proposed oxyanion intermediate. Dashed black lines show the coordination of Zn^{2+} and the hydrogen bonding network. Adapted with permission from [45]. Copyright 2014, Royal Society of Chemistry.

6.2. 2,6-Dihydroxybenzoate Decarboxylase from Polaromonas sporomusa JS666

Very recently Almo, Himo, and Raushel have solved the crystal structure of 2,6-dihydroxybenzoate decarboxylase (also called γ-resorcylate decarboxylase, γ-RSD) from *Polaromonas sporomusa* JS666 complexed with a 2-nitroresocinol inhibitor to a 1.65 Å resolution [54]. To date, only the thermodynamically favored 2,6-dihydroxybenzoate decarboxylation reaction catalyzed by the enzyme has been studied. The quaternary structure of the enzyme is a homotetramer. Each subunit consists of a distorted $(\alpha/\beta)_8$-barrel protein fold with the Mn^{2+} cation located at the C-terminal end of the barrel.

Figure 12 represents the active site structure of γ-RSD from *Polaromonas sporomusa* JS6666 showing the Mn^{2+} cation instead of the Zn^{2+} cation found in 2,6-DHBD from *Rhizobium sporomusa*

MTP-10005 [74]. From three-dimensional structure alignments, the two enzymes show a 77% amino acids identity. A recently characterized enzyme, 5-carboxy vanillate decarboxylase (LigW), from *Sphingomonas paucimobilis* (see Sections 5.4 and 6.4) shows a 37% amino acids identity with γ-RSD and, in analogy with γ-RSD, coordinates a Mn^{2+} cation in the active site.

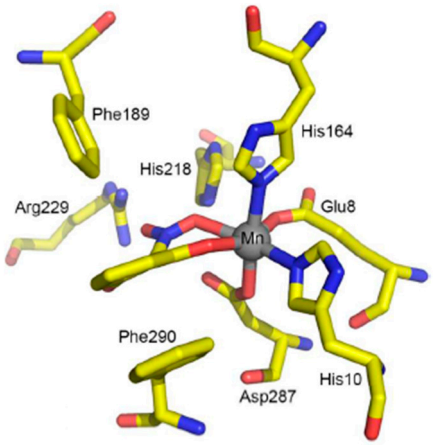


Figure 12. Active site structure of γ-RSD from *Polaromonas sporomusa* JS6666 (coordinating the 2-nitroresocinol inhibitor) showing the Mn^{2+} cation coordinated in an octahedral geometry. Reprinted with permission from [54]. Copyright 2018, American Chemical Society.

As shown in Figure 12, the Mn^{2+} cation is octahedrally coordinated by Glu8 and His10 (two amino acids from the β-strand 8), and His164 (from β-strand 5) and Asp287 (from β-strand 8). The coordination environment is completed by the nitro-group of the inhibitor and the adjacent phenolic oxygen. Figure 12 shows additionally Arg229 (an amino acid of the adjacent subunit) located within 3.2 Å from one of the oxygen atoms of the nitro-group of the 2-nitroresocinol inhibitor. Notably, the geometry of the 2-nitroresocinol deviates significantly from planarity. This feature is shared also by the phenolic substrate bound to Mn^{2+} in the 5-carboxy vanillate decarboxylase (LigW) enzyme (see Section 6.4).

Figure 13 presents the active site model coordinating γ-resorcylate (represented in orange color) instead of the nitro-resorcinol inhibitor. The main feature of the model is that the γ-resorcylate binds the Mn^{2+} cation as a di-anion and in a bidentate chelating coordination mode.

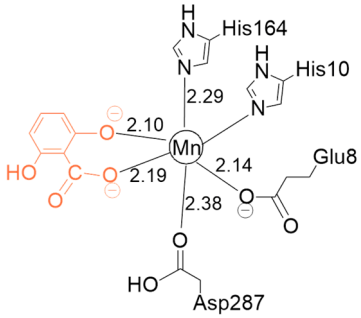


Figure 13. Scheme representing the coordination environment around the Mn^{2+} cation with resorcylate anion in a bidentate chelating coordination mode. Adapted with permission from [54]. Copyright 2018, American Chemical Society.

Structure of E:S (enzyme-substrate) and E:P (enzyme-product) complexes besides the structure of the proposed intermediate complex (Int) are shown in Figure 14. The authors propose the 2,6-dihydroxybenzoate decarboxylation reaction starts with protonation at the C1 atom of the substrate by Asp287, forming an intermediate (Int in Figure 14), which undergoes C-C bond cleavage and subsequent

re-aromatization of the ring, thus affording an Mn^{2+}-bound resorcinolate anion (E:P structure in Figure 14). The proposed mechanism was analyzed by density functional calculations (Figure 14) that allowed for an evaluation of the activation energy barrier (TS1, 14.8 kcal/mol) to reach the C1-protonated intermediate (Int). In turn, Int was calculated as lying 8.1 kcal/mol higher in energy with respect to the E:S complex.

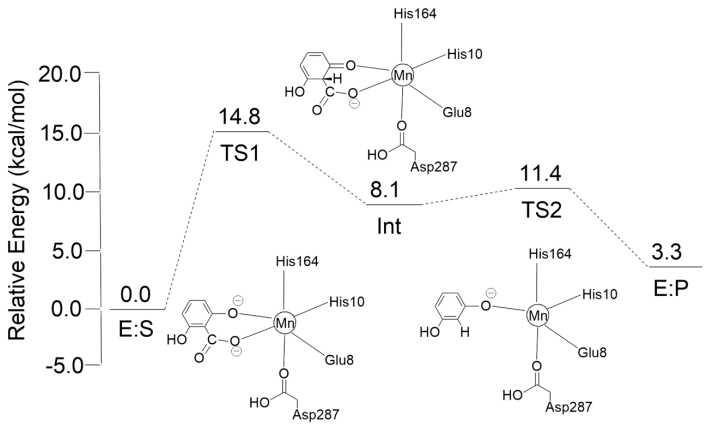


Figure 14. Structures of E:S (enzyme-substrate) complex, E:P (enzyme-product) complex, and Int (intermediate) complex. Calculated energy profile for the proposed reaction mechanism. Reprinted with permission from [54]. Copyright 2018, American Chemical Society.

Evolution of the intermediate Int into the E:P complex seems to be favored as TS2 have a relative energy of 11.4 kcal/mol as compared to E:S.

Almo and coworkers have also reanalyzed the reaction mechanism proposed by Goto and coworkers for γ-resorcylate decarboxylase (γ-RSD) from *Rhizobium* sp. By building up a reaction model in which the E:S-Zn complex (Figure 15) bears 2,6-dihydroxybenzoate bonded in a mono-dentate mode with C2-hydroxyl group engaged in hydrogen bonding with Asp287, the authors proposed that the E:S-Zn complex may evolve through Int1-Zn or Int2-Zn to yield either a resorcinol or resorcinol anion product.

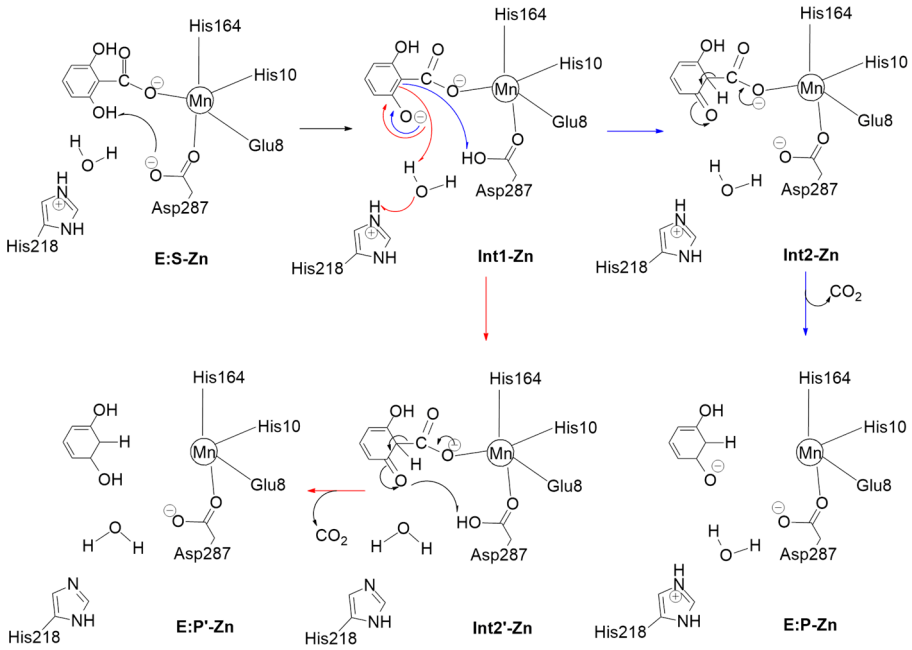


Figure 15. Possible reaction mechanisms for γ-RSD (from *Rhizobium* sp.) as proposed by Almo and coworkers. Orange curly arrows in Int1-Zn show the movement of electron pairs affording Int2′-Zn. Blue curly arrows in Int1-Zn show the movement of electron pairs affording Int2-Zn. Adapted with permission from [54]. Copyright 2018, American Chemical Society.

By Density Functional Theory (DFT analysis, it was calculated Int1-Zn lay19.2 kcal/mol higher with respect to E:S-Zn energy. Also, for Int2-Zn, a relative energy of 23.1 kcal/mol was calculated as compared to E:S-Zn energy. Based on these prohibitively high energy barriers, the authors concluded that the 2,6-dyhydroxybenzoate binding mode shown in the active site crystal structure reported by Goto and coworkers is probably not the productive mode for catalysis.

6.3. Salicylic Acid Decarboxylase from Trichosporon moniliiforme

As mentioned in Section 5.3, Ienaga and coworkers succeeded in obtaining a salicylic acid decarboxylase mutant with high specific activity toward the *meta*-amino phenol substrate [70].

As the wild-type salicylic acid decarboxylase from *Trichosporon moniliiforme* showed a 40% amino acid sequence identity with 2,6-dihydroxybenzoic acid decarboxylase from *Rhizobium sporomusa*, a SWISS MODEL [75] was used to build up a 3D model of the active site cavity of the two enzymes based on the crystal structure solved by Goto and coworkers. Moreover, 2,6-dihydroxybenzoate was docked into the active site cavity (Figure 16).

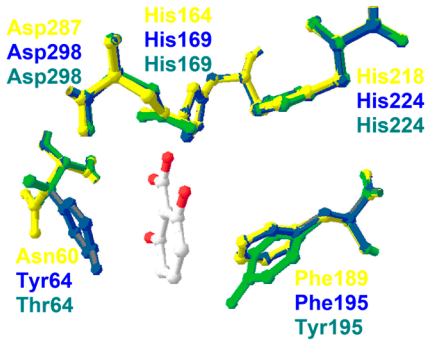


Figure 16. 3D structure of the 2,6-dihydroxybenzoic acid decarboxylase active site cavity showing, in yellow color, the relevant amino acids of the enzyme isolated from *Rhizobium sporomusa*. [74] The figure also shows: i) In blue color, the predicted amino acids of salicylic acid decarboxylase isolated from *Trichosporon moniliiforme* [68]; ii) in green color, the predicted amino acids of the double mutant-salicylic acid decarboxylase [70]. 2,6-dihydroxybenzoate (represented in white color) is docked into the cavity. Adapted with permission from [70]. Copyright 2013, The Chemical Society of Japan.

The model evidences that the double-mutant (Y64T-F195Y) bears Thr64 and Tyr195 (in green color) (corresponding to Asn60 and Phe189 in 2,6-dihydroxybenzoic acid decarboxylase from *Rizobium sporomusa*, in yellow color) in proximity to the entrance of the cavity. It is of note that the molecular weight of Thr64 is lower than Tyr64 and this is suggested to play an important role in enhancing the carboxylation activity toward *meta*-aminophenol. Concerning the hydroxyl group of Tyr195 of the double-mutant, the interaction with the amino group of *meta*-aminophenol is expected to play a key role in protein stabilization.

6.4. 5-Carboxyvanillate Decarboxylase from Sphingomonas paucimobilis SYK-6

Sphingomonas paucimobilis SYK-6 was isolated as a strain able to mineralize various lignin-derived biaryls [71]. This microorganism was shown possessing two genes encoding for two enzymes catalyzing the decarboxylation of 5-carboxyvanillate to vanillate that were named LigW_Sp and LigW2_Sp. Section 5.4 discusses the use of LigW_Sp and LigW2_Sp enzymes in the carboxylation reaction of representative lignin alcohols. Very recently, the crystal structure of LigW from *Sphingomonas paucimobilis* SYK-6 was determined as a resolution of 1.83 Å [58]. The protein is a 32-mer, where each subunit has a relative molecular mass of 38 kDa and consists of a central distorted $(\alpha/\beta)_8$-barrel domain with the active site located at the C-terminal end of the β-barrel.

Figure 17 shows the structure of the active site of the LigW enzyme from *Sphingomonas paucimobilis* SYK-6 containing an Mn^{2+} cation coordinated by His173, Glu7, Asp296, and one water molecule (Wat3).

The octahedral coordination sphere is completed by the 5-nitrovanillate inhibitor (represented in grey color) bound to the metal ion through the nitro- and the hydrohyl-group. Interestingly, Asp296 is part of a triad with His226 and Glu229. To date, mechanistic studies concerning LigW catalysis have aided in understanding the mechanism of the 5-carboxy vanillate decarboxylation reaction [58,59]. Currently, there is no mechanistic information on the reverse carboxylation reaction.

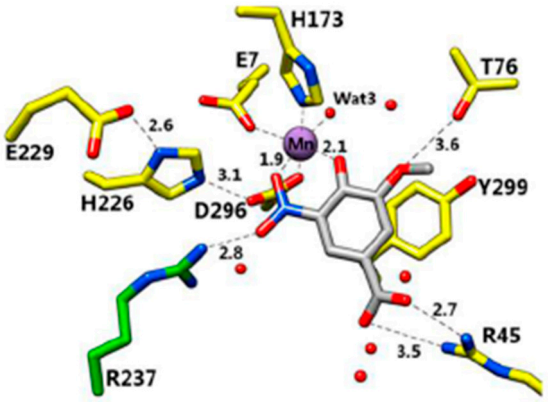


Figure 17. Structure of the active site of the LigW enzyme from *Sphingomonas paucimobilis* SYK-6 containing a Mn^{2+} cation in an octahedral environment. Reproduced with permission from [58]. Copyright 2016, American Chemical Society.

7. Insights into the Reaction Mechanism of 2,6-Dihydroxybenzoate Decarboxylase from *Rhizobium sporomusa*: Kinetic Studies

A detailed kinetic study was performed by Faber and coworkers [43] to determine kinetic parameters for catechol carboxylation to 2,3-dihydroxybenzoate (the reaction is shown in Table 2, entry 2).

The enzyme was over-expressed in *E. coli* and subsequently purified by using a nickel-NTA-agarose packed column. Solutions containing 0.2–0.3 mg of purified protein/mL were contacted with 2 M $KHCO_3$ and catechol at substrate concentrations ranging from 10 to 200 mM. Classical double-substrate Michaelis-Menten plots were obtained operating at pH = 8.3 and 30 °C, with the substrate concentration varying over the range 0–120 mM. In the experiments, a stoichiometric amount of ascorbic acid was added with respect to catechol to prevent substrate oxidation. Kinetic characteristics were calculated as: K_M of 30 ± 3 mM for catechol, V_{max} of 0.35 ± 1.1 10^{-2} μmol min^{-1} mg^{-1} for the carboxylation reaction, and k_{cat} of 0.12 ± 3.0 10^{-3} s^{-1}.

However, kinetic plots evidenced also that at high substrate concentrations (higher than 120 mM), the enzyme activity decreased significantly. These results could be explained as being due to protein deactivation. Considering the aforementioned study reported by Kirimura and coworkers [70] using a double-mutant of salicylic acid decarboxylase from *Trichosporon moniliiforme* WU-0401, one might expect that a similar directed mutagenesis study may allow for improved stability and catalytic activity of other carboxylase enzymes.

To calculate the K_M for $KHCO_3$ substrate, protein solutions containing 0.3–0.4 mg of protein/mL were loaded with catechol (100 mM) and $KHCO_3$ at concentrations ranging from 0 to 3 M. Solutions were tamponated at pH = 8 with a potassium phosphate buffer and incubated at 30 °C. From double-substrate Michaelis-Menten plots, a K_M of 839 ± 4 mM was found for HCO_3^-.

Study of the catechol carboxylation reaction under steady-state conditions allowed for the calculation of an equilibrium constant of 1.6 10^{-4} ± 8 10^{-6} M^{-1} (at 30 °C), corresponding to ΔG° = 5.2 ± 0.03 kcal/mol. The maximum catechol conversion into 2,3-dihydroxybenzoate under steady state conditions was 23%.

The obtained kinetic data were validated by comparison with predefined kinetic equations for reversible bi-uni reactions, where catechol and HCO_3^- bind to the active site in a random sequence.

Linear free-energy relationships (LFERs) analysis of the substrate scope of 2,3-dihydroxybenzoic acid decarboxylase from *Aspergillus oryzae* was used for mechanism investigation [76]. Although the reaction mechanism of 2,3-dihydroxybenzoic acid decarboxylase from *Aspergillus oryzae* is not known, its substrate scope is considerably larger if compared to the limited range of substrates carboxylated by 2,6-dihydroxybenzoic acid decarboxylase from *Rhizobium sporomusa*. Therefore 2,3-DHBD_Ao was considered suitable for an LFERs study. Twelve different di-substitited aromatic substrates with only one OH-substituent (except for catechol) were carboxylated by the enzyme and the *para*- or *meta*-effect of the X-substituent was referred to the carboxylic directing group (Figure 18) [76].

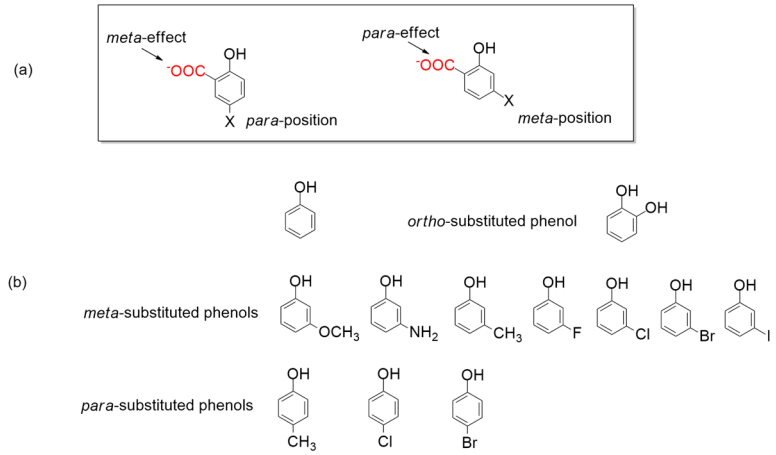


Figure 18. (**a**) The *meta*- or *para*-effect of the X-substituents was referred to the carboxylic directing group; (**b**) *ortho*-, *meta*-, and *para*-substituted phenols used in LFERs study.

The carboxylation reactions were carried out in HPLC screw-capped glass vials with *E. coli* whole lyophilized cells transformed with the 2,3-DHBD_Ao enzyme according to the following reaction conditions: 10 mM substrate, 30 mg/mL whole cells expressing 2,3-dihydroxybenzoic acid decarboxylase from *Aspergillus oryzae* (2.1 U/mL), 3 M $KHCO_3$, and 30° (the activity of the carboxylase enzymes was determined using catechol as the substrate).

The apparent equilibrium constants ($K_{eq,app}$) for the carboxylation reaction of different substrates shown in Figure 18 were calculated and the log($K_{eq,app}$) was correlated with respect to the pertinent Taft constants (σ^0) (Figure 19).

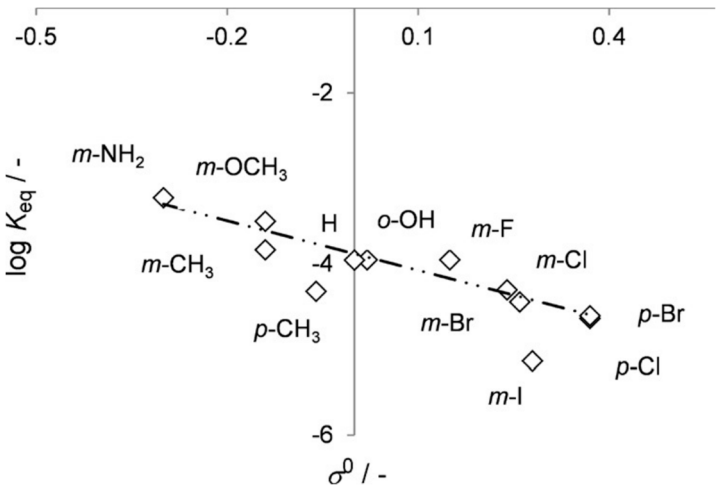


Figure 19. Correlation of the logarithm of the calculated $K_{eq,app}$ with respect to the Taft constants (σ^0) for substrates shown in Figure 18, (R^2 = 0.93). Reprinted with permission from [76]. Copyright 2016, John Wiley and Sons.

A linear correlation was found for 10 out of the 12 substrates investigated. The linearity observed for substrates bearing both *para*- and *meta*-X-substituents suggests that various regio-isomers do not influence the reactions (except for *para*-CH_3 and *meta*-I). More importantly, the negative slope ($\rho = -1.9$) indicates that the reaction is favorable when the reactive center (the carbon anion at the *ortho*-position with respect to the -OH substituent) is electron rich. This result is in accordance to the reaction mechanism proposed for the Kolbe-Schmitt reaction.

In a parallel study, the initial reaction rates (v) for the carboxylation reaction of eight different substrates were measured according to the following reaction conditions: Substrate 10 mM, 30 mg/mL whole cells expressing Ao_DHBD (2.1 U/mL), in 3 M $KHCO_3$, 30 °C. The log$v$ was correlated with respect to the pertinent Taft constants, σ^0 (Figure 20).

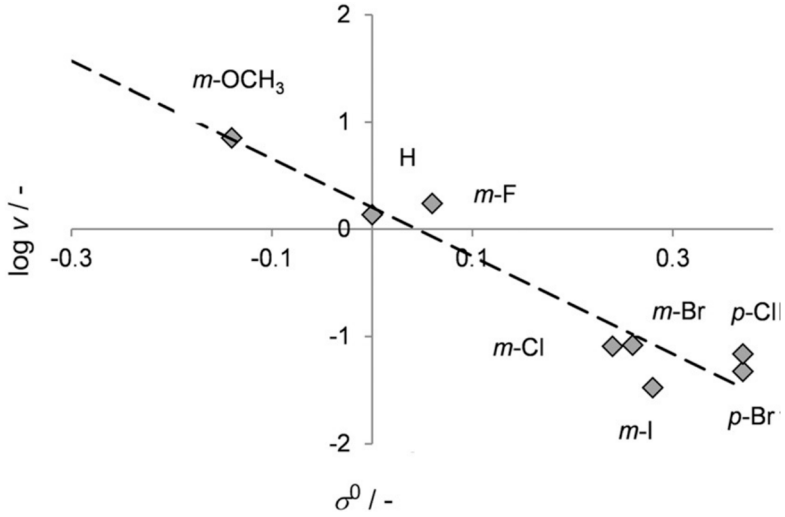


Figure 20. Correlation of the logarithm of the calculated initial reaction rates (v) with respect to the Taft constants (σ^0) for the selected set of substrates shown in Figure 18, ($R^2 = 0.92$). Reprinted with permission from [76]. Copyright 2016, John Wiley and Sons.

Also, in this case, a negative slope ($\rho = -4.5$) is expected (and observed) for a reaction mechanism involving a nucleophilic center.

Overall, the LFERs study allowed the authors to ascertain that the reaction mechanism of the 2,3-DHBD_Ao enzyme can be classified as electrophilic aromatic substitution/water elimination with HCO_3^- as a co-substrate.

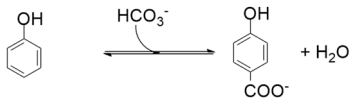
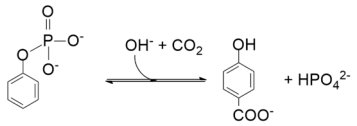
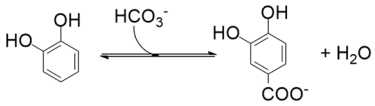
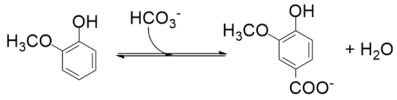
8. Regioselective Enzymatic *Para*-Carboxylation of Phenols: The Enzymes' Reactivity

Several enzymes catalyzing reversible 4-hydroxybenzoate, 3,4-dihydroxybenzoate, and 4-hydroxy-3-methoxybenzoate decarboxylation have been purified from various strict and facultative anaerobic bacteria (Table 9) [47]. For each enzyme, the representative carboxylation reaction is shown. Only the enzymes that have been shown to catalyze the thermodynamically unfavorable carboxylation reaction have been considered in the list.

In fermenting strict anaerobes (entry 1), the substrate is directly carboxylated using CO_2 provided high concentrations of phenol and CO_2 (or HCO_3^-) are used and 4-hydroxybenzoate is efficiently removed from the equilibrium.

In facultative aerobes, like denitrifying and phototrophic bacteria (entry 2), phenol is carboxylated regioselectively to 4-hydroxybenzoate, however, the carboxylation reaction requires a prior activation of phenol to phenylphosphate.

Table 9. List of decarboxylase enzymes catalyzing the regioselective *para*-carboxylation reaction of hydroxyl aromatic substrates recently characterized.

Entry	Enzyme	Microorganism	Reference
1	4-hydroxybenzoate decarboxylase 	*Enterobacter cloacae* P240 *Clamidophila pneumonia* AR39 *Clostridium*-like bacterium	[77] [78] [79]
2	phenylphosphate carboxylase 	*Thauera aromatica* K172 *Desulfatiglans anilini* *Rhodopseudomonas palustris*	[80,81] [82] [83]
3	3,4-dihydroxybenzoate decarboxylase 	*Enterobacter cloacae* P241 *Clostridium hydroxybenzoicum* JW/Z-1T	[84] [85]
4	4-hydroxy-3-methoxybenzoate decarboxylase (fermenting anaerobes) 	*Bacillus subtilis* ATCC6051	[86]

8.1. Regioselective Para-Carboxylation of Phenol by 4-Hydroxybenzoate Decarboxylase from Enterobacter cloacae P240

Nagasawa and coworkers have reported in 2006 the purification and characterization of a 4-hydroxybenzoate decarboxylase enzyme from *Enterobacter cloacae* P240 (representative reaction is shown in Table 9, entry 1) [77]. Enzymatic activity was measured in potassium phosphate buffer solutions (pH = 7, 100 mM) containing the purified protein or whole cells loaded with phenol (20 mM) and $KHCO_3$ (3 M). 10 mM of dithiothreitol was added to prevent protein oxidation and the solution was incubated at 20 °C. Formation of 4-hydroxybenzoate was observed in 19% conversion.

Other enzymes, such as 4-hydroxybenzoate decarboxylase from *Chlamydophila pneumonia* AR39 [78] and from a *Chlostrium*-like strain [79], were reported to produce low amounts of 4-hydroxybenzoate when incubated using similar methods.

8.2. Regioselective Para-Carboxylation of Phenol by Phenylphosphate Carboxylase from Thauera aromatica K172

The carboxylation reaction of phenol to 4-hydroxybozoate has been extensively studied in the nitrate reducing bacteria, *Thauera aromatica* K172 [47,80,81], which was shown to possess an operon of at least 15 genes involved in phenol carboxylation.

In *Thauera aromatica*, the phenol is at first phosphorylated to phenylphosphate by a phenylphosphate synthase (Figure 21a). Subsequently, phenylphosphate is cleaved and carboxylated by phenylphosphate carboxylase (Figure 21b). It is of note that phenyphosphate carboxylase is specific for CO_2 more that HCO_3^-. Phenylphosphate carboxylase is composed of four subunits (α,β,γ,δ, Figure 21c). The δ subunit seems to be responsible for the cleavage of phenylphosphate by OH^- to yield HPO_4^{2-} and a phenoxide anion (Figure 21c), which is transferred to the α,β,γ subunits and finally regioselectively carboxylated to 4-hydroxybenzoate.

The hydrolysis of one mole of ATP for phenylphosphate synthesis makes the overall carboxylation reaction thermodynamically favored. According to Fuchs, phenol phosphorylation is required to favor phenol trapping inside the cell. As phosphate is a deactivating group for the aromatic

ring carboxylation, it must be removed, allowing the formation of a phenoxide anion that undergo carboxylation with CO_2.

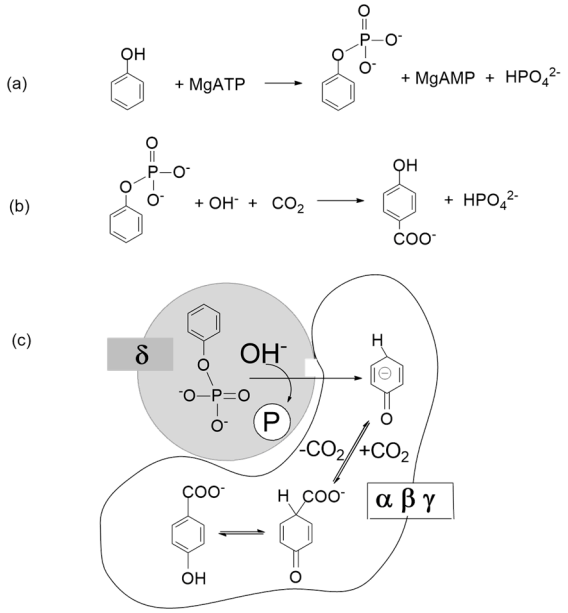


Figure 21. (**a**,**b**) Reactions catalyzed by phenylphosphate synthase and phenylphosphate carboxylase in *Thauera aromatica*; (**c**) schematic represention of the α,β,γ,δ subunits of phenylphosphate carboxylase. Adapted with permission from [47]. Copyright 2009, Springer Nature.

Very recently, the genes encoding for phenylphosphate synthase and phenylphosphate carboxylase were also found in the sulphate-reducing bacterium, *Desulfatiglans anilini* [82].

8.3. Regioselective Para-Carboxylation of Phenol by 3,4-Dihydroxybenzoate Decarboxylase from Enterobacter cloacae P241

Nagasawa and coworkers reported in 2010 the induction of a 3,4-hydroxybenzoate decarboxylase enzyme from *Enterobacter cloacae* P241 (the representative reaction is shown in Table 9, entry 3) [84]. Enzyme solutions containing cell extracts were suspended in a potassium phosphate buffer (pH = 7, 10 mM) and loaded with catechol (50 mM) and $KHCO_3$ (3 M). 5 mM of dithiothreitol and 20 mM of $Na_2S_2O_3$ were added to prevent protein oxidation and the solution was incubated at 30 °C during 14 h. 3,4-hydroxybenzoate was obtained with 28% conversion. Previous work reported by Wiegel and coworkers by using purified 3,4-hydroxybenzoate decarboxylase from *Clostridium hydroxybenzoicum* JW/Z-1T afforded 3,4-hydroxybenzoate with approximately 16% conversion [85].

8.4. Regioselective Para-Carboxylation of Guaiacol by Vanillate Decarboxylase from Bacillus subtilis ATCC 6051

Wiegel and coworkers have characterized a decarboxylase enzyme specific for 4-hydroxybenzoate and 3-methoxy-4-hydroxybenzoate (vanillate) substrates in *Bacillus subtilis* ATCC 6051 [86]. The genes encoding for the enzyme were cloned in *E. coli* and the activity of the enzyme was studied both in *Bacillus subtilis* and in *E. coli* recombinant cells. To study the uphill carboxylation reactions (see the representative reaction in Table 9, entry 4), crude extract proteins from the two microorganisms were incubated with phenol or guaiacol (15 mM) and $NaHCO_3$ (100 mM) at 37 °C during 1 h. Measured specific activities for the carboxylation of phenol and guaiacol using the protein expressed in *E. coli* were 0.6 ± 0.2 U/mg of protein and 0.5 ± 0.1 U/mg of protein, respectively. Using the native decarboxylase enzyme from *B. subtilis*, guaiacol was carboxylated with a maximum specific activity of 0.9 ± 0.2 U/mg of protein.

9. Para-Hydroxystyrenes β-Carboxylation by Phenolic Acid Decarboxylase (PAD) Enzymes

Faber et al. have recently reported a biocatalytic approach for the regioselective and (E/Z)-stereoselective carboxylation of *para*-hydroxystyrenes to (*E*)-4-hydroxycinnamic acid derivatives with HCO_3^- as the CO_2 source using phenolic acid decarboxylase enzymes (PAD). The authors claim that the carboxylation reaction shown in Figure 22 does not find a direct counterpart in chemical synthetic reactions [87,88].

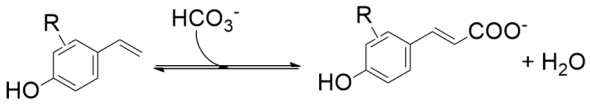
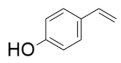
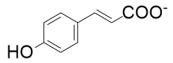
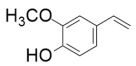
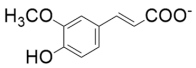
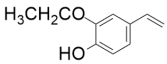
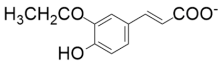
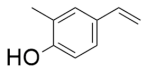
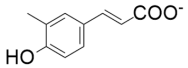
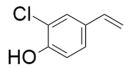
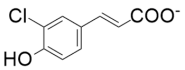
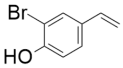
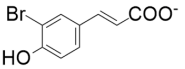
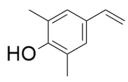
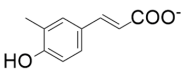
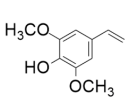
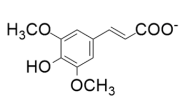


Figure 22. (E/Z)-stereoselective carboxylation of *para*-hydroxystyrenes to (*E*)-4-hydroxycinnamic acids derivatives using phenolic acid decarboxylase enzymes (PAD).

In nature, phenolic acids decarboxylases catalyze the decarboxylation reaction of ferulic, caffeic, coumaric, and sinaptinic acids, which are synthesized by cells via oxidative biodegradation of lignin. In a previous work [88], Faber and coworkers used phenolic acids decarboxylases from *Lactobacillus plantarum* and *Bacillus amyloliquefaciens* to promote the reverse carboxylation of *para*-vinylphenol and 2-methoxy-4-vinylphenol to *para*-coumaric and ferulic acids by using HCO_3^- at a concentration of 3 M. The carboxylate products were obtained with a low to moderate yield (2–30%). By using phenolic acid decarboxylases from *Mycobacterium colombiense*, *Methylobacterium* sp., *Pantoea* sp., *Lactococcus lactis*, and ferulic acid decarboxylase from *Enterobacter* sp., Faber succeeded in the carboxylation of a wide range of *para*-hydroxystyrene derivatives (Table 10). As a standard procedure, the genes of the enzymes were synthesized and subcloned in *E. coli* BL21(DE3). Subsequently, lyophilized whole cells (30 mg) overexpressing the enzymes were suspended in a phosphate buffer (pH 8.5, 100 mM) and incubated in the presence of the substrate (10 mM) and $KHCO_3$ (3 M), at 30 °C during 24 h. Additionally, acetonitrile at 20% *v*/*v* was used.

Table 10. Scope of the carboxylation reaction of *para*-hydroxystyrene derivatives by PAD. Reproduced with permission from [87]. Copyright 2015, John Wiley and Sons.

Entry	Substrate	Product	PAD_Mc Conversion (%)	PAD_Ps Conversion (%)	PAD_LI Conversion (%)
1			18	17	3
2			28	20	2
3			11	35	35
4			28	13	1
5			30	18	26
6			18	<1	<1
7			26	14	10
8			1	5	4

β-carboxylated products were obtained with conversion up to 35%. The activating *para*-hydroxy group was required for the enzymes to catalyse the reaction while the substitution at the α- or β-position of the vinyl-substituent was detrimental (data not shown in Table 10).

Based on molecular modelling studies based on the crystal structure of ferulic acid decarboxylase from *Enterobacter* sp. [89], the following reaction mechanism (Figure 23) was proposed: The substrate is oriented into the active site with the hydroxyl group close to Tyr19. HCO_3^- strongly interacts through a salt bridge and H-bonds with Arg49. The Tyr19 amino acid residue, which is activated, in turn, from Tyr21, is engaged into hydrogen abstraction from the substrate. The substrate anion delocalizes the electron density through the aromatic core to the C-β carbon of the alkene moiety, which nucleophilically attacks HCO_3^-. It thus forms a charge-stabilized quinone-methyde oxyanion intermediate (shown in Figure 23). Successive water elimitation restores the aromaticity. As can be noted in Figure 23, neither metal cations nor a cofactor is involved in catalysis.

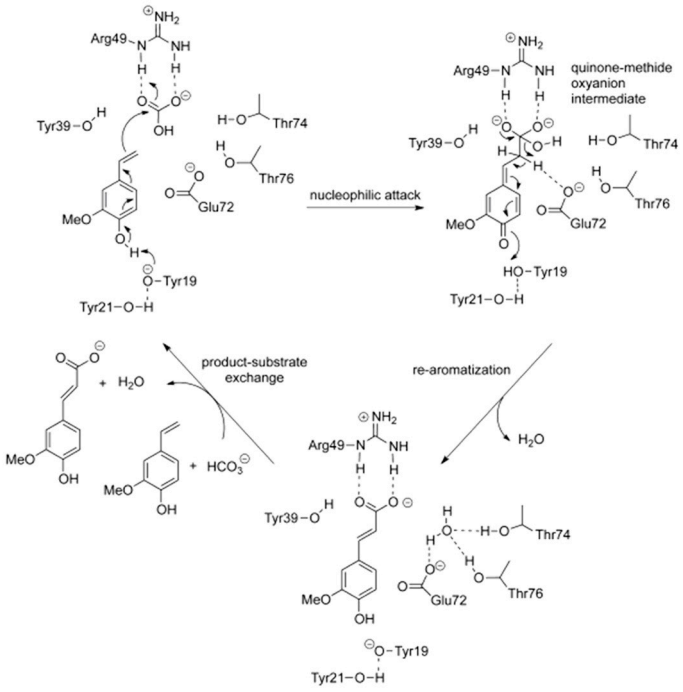


Figure 23. Proposed reaction mechanism for carboxylation of *para*-hydroxystyrene from PAD. Reproduced with permission from [87]. Copyright 2015, John Wiley and Sons.

More recently, Himo and coworker performed a DFT analysis of the optimized active site structure of PAD from *Bacillus substilis* [90]. The calculated energy profile for the carboxylation of *para*-vinylphenol to cinnamic acid suggests that the nucleophilic β-carbon atom of the vinyl-group attacks a CO_2 molecule rather than HCO_3^-. CO_2 is proposed to form through protonation of HCO_3^- by Glu 64, causing H_2CO_3 decomposition to CO_2 and H_2O.

Ferulic acid decarboxylase enzyme (FDC) is currently used to promote decarboxylation reactions of a wide range of acrylic acid derivatives, yielding terminal alkenes with a conversion up to 99% [91].

10. Enzymatic Carboxylation of Aromatic Hydrocarbons

Although the aerobic pathways for benzene microbial degradation are well studied, benzene degradation in an anaerobic environment deserves further investigations. Three putative reactions have been proposed for benzene activation (Figure 24a) in anaerobic bacteria: Hydroxylation to phenol, direct carboxylation to benzoate, and methylation to toluene [92].

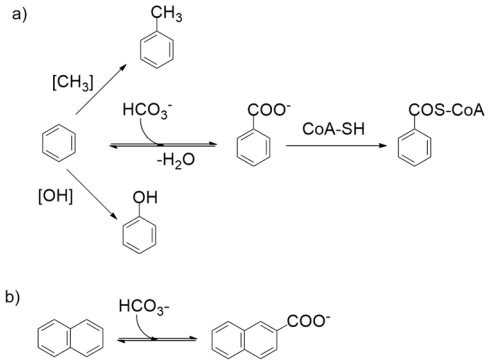


Figure 24. Putative anaerobic degradation pathways of benzene (**a**) and naphthalene (**b**).

A recent study reported by Atashgahi and coworkers [93] appears to confirm the results of previous studies reported by Meckenstock and coworkers [94] indicating the presence of a gene cluster encoding for proteins potentially involved in direct benzene carboxylation in *Peptococcaceae* family [93]. In particular, the gene cluster consists of: *ubiD* gene encoding for the benzene carboxylase, AbcD subunit, *ppcC* gene encoding for the benzene carboxylase large subunit, AbcA), and *bzlA* gene encoding for the benzoate-CoA ligase protein.

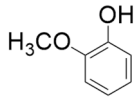
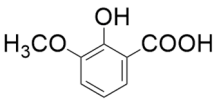
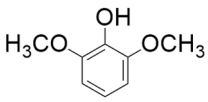
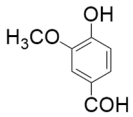
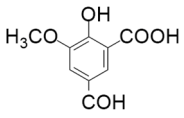
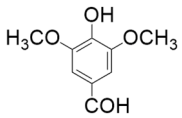
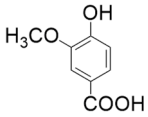
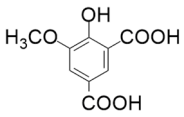
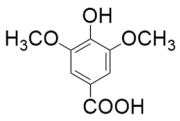
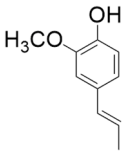
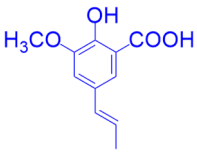
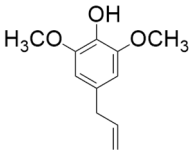
As far as the recalcitrant polycyclic aromatic hydrocarbon naphthalene is concerned, the metabolite analysis of sulfate reducing enrichment culture N47 supernatant indicates the substrate degradation being initiated by carboxylation (to form 2-naphthalene carboxylate, Figure 24b) or methylation reactions [95]. To confirm the origin of the carboxylic group in 2-naphthalene carboxylate, cultures were grown using [^{13}C]-hydrogencarbonate as a medium buffer incorporating the ^{13}C label into the carboxyl group of 2-naphthalene carboxylate.

In crude cell extracts of the sulfate reducing enrichment culture N47, a naphthalene carboxylase enzyme converting naphthalene and ^{13}C-labelled hydrogencarbonate into 2-[*carboxyl*-^{13}C]-naphthalene carboxylate was identified. The naphthalene carboxylate was produced at a rate of 0.12 nmol/ min mg protein.

11. Enzymatic Carboxylation Reactions Open the Perspective for Valorization of Lignin-Derived Aromatics.

To analyze the possible contribution of the abovementioned carboxylation reactions to the valorization of lignin-derived aromatics, the most representative monomeric phenolic compounds obtained by conventional chemical and physico-chemical treatment of lignocellulosic materials (as exemplified in Table 2) are shown in Table 11 [21–26]. These compounds are essentially guaiacol (column A, Table 11) and syringol derivatives (column C, Table 11). Catechol is also obtained in the ECN fast pyrolysis process cited in Table 2 [22], although in a very low yield. Due to the free *ortho*-position (with respect to the -OH directing group), guaiacol-derivatives shown in column A are suitable substrates for decarboxylase enzymes as 2,3-DHBD_Ao, 2,3-DHBD_Fo, 2,6-DHDB_Rs, and SAD_Tm, and also for LigW_Sp and LigW2_Sp decarboxylases. In particular, some carboxylated products shown in Table 11 (entries 1–3) have been obtained as products of enzymatic carboxylation reactions analyzed in previous Sections (see for example: Table 6, entry 5; Table 4, entry 1; Table 8, entry 3). The product shown in entry 4 (column B) has not been reported as being obtained by *ortho*-carboxylation of 2-methoxy-4-(prop-1-en-1yl)phenol ((*E*)-isoeugenol), although its very close structural analog, 2-methoxy-4-propylphenol, has been converted into 2-hydroxy-3-methoxy-5-propylbenzoic acid by LigW_Sp decarboxylase (see Table 8, entry 2).

Table 11. Column A and C show the monomeric hydroxyaromatic compounds obtained from chemical and physico-chemical treatment of lignin analyzed in Table 2. Column B shows the *ortho*-carboxylated products of guaiacol-derivatives obtained by an enzymatic carboxylation reaction (the *ortho*-carboxylated product shown in entry 4 has not been reported in the literature, therefore, it is presented in blue color).

Entry	Column A Guaiacol and Guaiacol Derivatives	Column B Carboxylated Products	Column C Syringol and Syringol Derivatives
1			
2			
3			
4			

The carboxylic acids shown in column B of Table 11 may find an application as building blocks in the synthesis of polyesters and polyamides [96]. However, it should be pointed out clearly that, at present, the guaiacol- and syringol-derivatives shown in Table 11 have been obtained in very low yields and selectivity by treatment of lignocellulosic material, therefore, their use is significantly limited.

It is of note that some very recent examples of lignin depolymerization processes affording monomeric phenols with good selectivity have been reported, showing that efficient lignocellulose deconstruction/depolymerization is feasible and will probably develop in the near future.

A recent work by Barta and coworkers [97] reports the synthesis of guaiacol-derivatives (shown in Figure 25a) from pine lignocellulosic material, without pretreatment, by using a Cu-doped porous metal-oxide catalyst (Cu_2O-PMO) [98] under H_2 (4 MPa) at 220 °C. The process allows for the obtaining of guaiacol-derivatives that are soluble in methanol solution and a cellulose rich-solid fraction that is subsequently processed and transformed into low molecular weight aliphatic compounds. The Cu-catalyst is easily recovered from the cellulose-solid fraction and fully recycled. Guaiacol-derivatives shown in Figure 25a are obtained in a total yield of 13% [Yield % = ($weight_{monomers}$/$weight_{lignin}$) × 100] with a selectivity to 4-hydroxy-3-methoxybenzenepropanol, 2-methoxy-4-propylphenol, and 4-ethyl-2-methoxyphenol of 61%, 33%, and 6%, respectively.

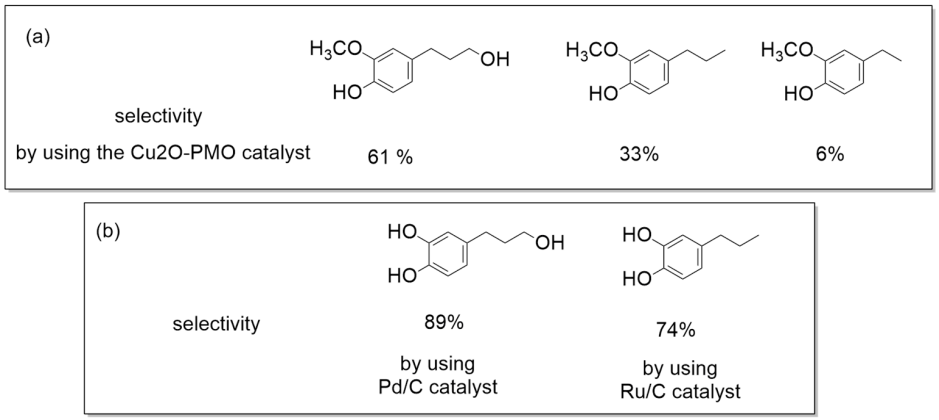


Figure 25. Monomeric phenols obtained with good selectivity by recently reported chemical treatment of lignocellulosic material. (**a**) guaicol derivatives; (**b**) catechol derivatives.

As mentioned in Section 2, vanilla seed coats containing C-lignin are easily converted by hydrogenolisis [29] in catechol-derivatives. Vanilla seeds are milled and extracted from polysaccharides by using CELLULYSIN cellulases, then 200 mg of the preextracted material is mixed with 30 mL of CH_3OH and 100 mg of Pd/C or Ru/C catalyst (5 wt.%) in a 100 mL high-pressure reactor, which is sealed and pressurized with H_2 (4 MPa). Hydrogenolysis is carried at 200 °C during 15 h. Interestingly, by using Pd/C and Ru/C catalysts in CH_3OH, almost a quantitative lignin conversion into hydroxyaromatic monomers was obtained. It is of note that the use of the Pd/C catalyst afforded 4-(3-hydroxypropyl)benzene-1,2-diol with an 89% selectivity while the use of Ru/C catalyst afforded 4-propylbenzene-1,2-diol with a 74% selectivity (Figure 25b).

To show how enzymatic carboxylation reactions may open a perspective for valorization of lignin-derived aromatics (Figure 26a), 2-methoxy-4-propylphenol can be converted into 2-hydroxy-3-methoxy-5-propylbenzoic acid by LigW_Sp decarboxylase (see Table 8, entry 2). By using synthetic biology tools, the carboxylated product could be further converted into 2,3-dihydroxy-5-propylbenzoic acid by a O-demethylase enzyme in a new biosynthetic pathway engineered in microbial hosts (Figure 26a). Making dihydroxybenzoic acid derivatives that possess the structure shown in Figure 26c is highly desirable as these compounds find applications as charging and dispersing agents for electrophoretic deposition (EPD) [99].

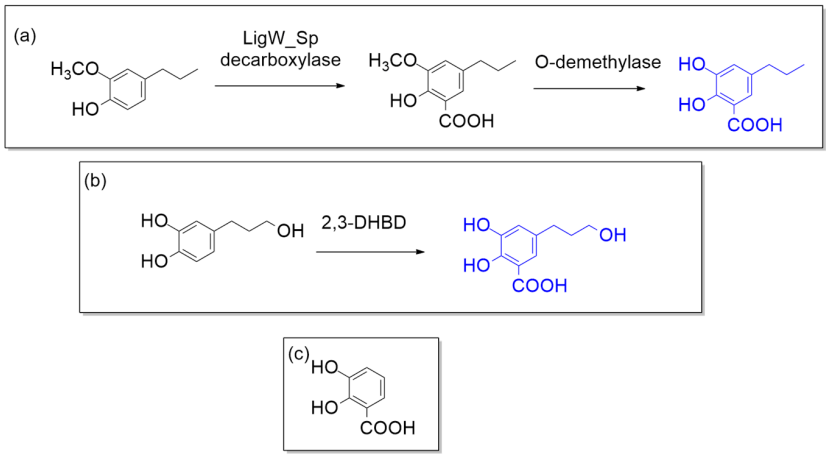


Figure 26. Possible role of the decarboxylase enzyme in the functionalisation of guaiacol- and catechol-derivatives to produce valuable compounds. Compounds in blue color could be obtained by using the synthetic biology technology. (**a**) carboxylation and O-demethylation of a guaiacol-derivative; (**b**) carboxylation of a catechol derivative; (**c**) 2,3-dihydroxybenzoic acid.

Considering catechol-derivatives shown in Figure 25b, further enzymatic processing to obtain hydroxybenzoic acid derivatives (Figure 26b) is also desirable for many applications [100].

Therefore, the use of robust and efficient decarboxylase enzymes may contribute a valuable synthetic tool to synthetic biology technology aimed at valorization of lignin-derived aromatics.

Also, problems related to the growth of bacterial cultures fed with phenols and hydroxybenzoic acids have been recently addressed and elegantly solved.

Thanks to recent advances in synthetic biology, *E. coli* has been transformed with a transporter (CouP) induced by a vanillin-promoter (ADH7), allowing the microorganism to grow at high concentrations of the aromatic compound (0.5 g of vanillin/L) and to carry out an engineered reaction pathway to produce catechol (up to 8 mg/L) within 10 h, as shown in Figure 27 [101].

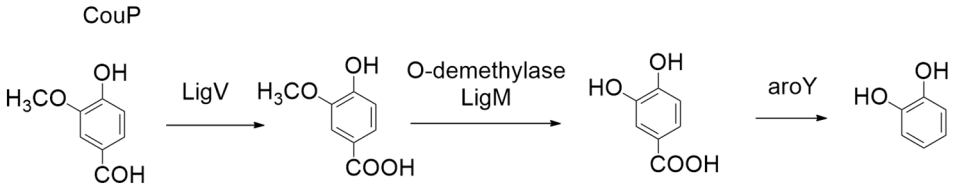


Figure 27. Engineered pathway wired in *E. coli* to produce catechol from vanillin. CouP = aromatic transporter; LigV = vanillin dehydrogenase; LigM = vanillate-O-demethylase; aroY = protocatechuate decarboxylase. Adapted with permission from [101]. Copyright 2018, Proceedings of the National Academy of Sciences of the United States of America.

12. Conclusions

The above reported literature analysis shows that studies concerning the catalytic activity of hydroxyaromatic acid decarboxylase enzymes have attracted the interest of the scientific community over almost three decades. Recently, the interest has grown significantly and new enzymes have been discovered and characterized, such as, for example, phenolic acid decarboxylase (PAD) from *Mycobacterium colombiense*, γ-resorcylate decarboxylase (γ-RSD) from *Polaromonas sporomusa* JS6666, and 5-carboxyvanillate decarboxylase form *Sphingomonas paucimobilis* SYK-6. The interest is mainly directed to finding more efficient enzymes that enable the valorization of hydroxyl aromatic compounds and polyphenols derived from lignin decomposition with the production of value added compounds.

Overall, the following main conclusions may be drawn:

1) 2,3-DHBD_Ao, 2,3-DHBD_Fo, 2,6-DHDB_Rs, SAD_Tm enzymes analyzed in the above Sections have been shown as being versatile enzymes able to functionalise with high regioselectivity a wide range of phenols to valuable *ortho*-hydroxybenzoic acids using HCO_3^- as a CO_2 source (see Tables 3, 4 and 6). However, due to thermodynamic constraints, the reaction must be carried out under CO_2 pressure or in the presence of quaternary ammonium salts to achieve high conversions (up to 97%).
2) 2,3-DHBD_Ao and 2,6-DHDB_Rs enzymes show better conversion (up to 97%) in the carboxylation of polyphenolic compounds (Tables 4 and 5) possessing the resorcinol moiety. Scaling up of the reaction has been shown to be feasible. As noticed by Faber, the carboxylation of polyphenols increases the stability of the molecule toward light-degradation. In addition, γ-resorcylic acids bearing a lipophilic substituent are known as thrombolytic and anti-inflammatory agents.
3) The newly discovered LigW_Sp and LigW2_Sp decarboxylase enzymes are able to carboxylate hydroxycinnamic acid derivatives as well as guaiacol-derivatives, with excellent selectivity toward *ortho*-carboxylation with respect to the -OH directing group. At the moment, they are the best candidates for targeting the valorization of lignin-derived aromatics through carboxylation reactions. Also, phenolic acid decarboxylase enzymes (PAD) are good candidates for lignin

valorization provided that *para*-hydroxystyrene derivatives can be efficiently recovered from natural lignin sources.

4) Enzymes catalyzing selective *para*-carboxylation of phenol, phenylphosphate, catechol, and guaiacol (with respect to the -OH directing group) summarized in Table 9 present a valuable tool for the synthesis of *para*-hydroxybenzoic acid derivatives.
5) Functionalisation of aromatic hydrocarbons as benzene and naphthalene is also a synthetically attractive procedure, although research in this specific field seems at a "nascent stage".
6) Advances in the structural and "kinetics" characterization of the enzymes will significantly contribute to elucidate the enzymatic reaction mechanism and to enhance the enzyme's performance through mutational studies.

Author Contributions: I.T., writing—original draft preparation.

Funding: This research and APC was funded by MIUR, Progetto di Ricerca Industriale e Sviluppo Sperimentale "TARANTO" (ARS01_00637).

Acknowledgments: The University of Bari Aldo Moro is acknowledged for its financial support (Fondi Ordinari di Supporto alla Ricerca 2015/2016).

Conflicts of Interest: The author declares no conflict of interest.

References and Note

1. Soekamto, N.H.; Islam, M.F. Phenetyl ester and amide of Ferulic Acids: Synthesis and bioactivity against P388 Leukemia Murine Cells, IOP Sciences. *J. Phys. Conf. Ser.* **2018**, *979*, 012016. [CrossRef]
2. Dasagrandhi, C.; Park, S.; Jung, W.-K.; Kim, Y.-M. Antibacterial and Biofilm Modulating Potential of Ferulic Acid Grafted Chitosan against Human Pathogenic Bacteria. *Int. J. Mol. Sci.* **2018**, *19*, 2157. [CrossRef]
3. Tomi, M.J.; Sharania, C.S.; Mahapatra, D.K.; Suresh, K.I.; Sabu, A.; Haridas, M. In vitro assessment of selected benzoic acid derivatives as anti-inflammatory compounds. *J. Sci. Ind. Res.* **2017**, *77*, 330–336.
4. Hawley, S.A.; Fullerton, M.D.; Ross, F.A.; Schertzer, J.D.; Chevtzoff, C.; Walker, K.J.; Peggie, M.W.; Zibrova, D.; Green, K.A.; Mustard, K.J.; et al. The Ancient Drug Salicylate Directly Activates AMP-Activated Protein Kinase. *Science* **2012**, *336*, 918–922. [CrossRef]
5. Furukawa, H.; Cordova, K.E.; O'Keeffe, M.; Yaghi, O.M. The Chemistry and Applications of Metal-Organic Frameworks. *Science* **2013**, *341*, 1230444. [CrossRef] [PubMed]
6. Barman, S.; Mukhopadhyay, S.K.; Behara, K.K.; Dey, S.; Singh, N.D.P. 1-Acetylpyrene−Salicylic Acid: Photoresponsive Fluorescent Organic Nanoparticles for the Regulated Release of a Natural Antimicrobial Compound, Salicylic Acid. *ACS Appl. Mater. Interfaces* **2014**, *6*, 7045–7054. [CrossRef]
7. Wang, Z.; Miller, B.; Mabin, M.; Shahni, R.; Wang, Z.D.; Ugrinov, A.; Chu, Q.R. Cyclobutane-1,3-Diacid (CBDA): A Semi-Rigid Building Block Prepared by [2+2] Photocyclization for Polymeric Materials. *Sci. Rep.* **2017**, *7*, 13704. [CrossRef] [PubMed]
8. Wiley-VCH Verlag GmbH & Co. KGaA. *Ullmann's Encyclopedia of Industrial Chemistry*, 2nd ed.; Carboxylic Acids, Aromatic; Wiley-VCH Verlag GmbH & Co. KGaA: Weinheim, Germany, 2005.
9. Lindsey, A.S.; Jeskey, A. The Kolbe-Schmitt reaction. *J. Chem. Soc.* **1957**, *57*, 583–620. [CrossRef]
10. Luo, J.; Preciado, S.; Xie, P.; Larrosa, I. Carboxylation of Phenols with CO_2 at Atmospheric Pressure. *Chem. Eur. J.* **2016**, *22*, 6798–6802. [CrossRef] [PubMed]
11. Feldman, A.W.; Romesberg, F.E. Expansion of the Genetic Alphabet: A Chemist's Approach to Synthetic Biology. *Acc. Chem. Res.* **2018**, *51*, 394–403. [CrossRef] [PubMed]
12. Lee, S.Y.; Kim, H.U. Systems strategies for developing industrial microbial strains. *Nat. Biotechnol.* **2015**, *33*, 1061–1072. [CrossRef] [PubMed]
13. Lutz, S.; Bornscheuer, U.T. *Protein Engineering Handbook*; Vol. 1 and Vol. 2; WILEY-VCH Verlag GmbH & Co. KGaA: Weinheim, Germany, 2009.
14. Kahl, L.J.; Endy, D. A survey of enabling technologies in synthetic biology. *J. Biol. Eng.* **2013**, *7*, 13. [CrossRef]
15. Chubukov, V.; Mukhopadhyay, A.; Petzold, C.J.; Keasling, J.D.; Martín, H.G. Synthetic and systems biology for microbial production, of commodity chemicals. *Syst. Biol. Appl.* **2016**, *2*, 16009. [CrossRef] [PubMed]
16. Ragauskas, A.J. The frontiers of Energy. *Nat. Energy* **2016**, *1*, 15020.

17. Rinaldi, R.; Jastrzebski, R.; Clough, M.T.; Ralph, J.; Kennema, M.; Bruijnincx, P.C.A.; Weckhuysen, B.M. Paving the way for lignin valorisation: Recent advances in bioengineering, biorefining and catalysis. *Angew. Chem. Int. Ed.* **2016**, *55*, 8164–8215. [CrossRef]
18. Ralph, J. Hydroxycinnamates in lignification. *Phytochem Rev.* **2010**, *9*, 65–83. [CrossRef]
19. Chena, F.; Tobimatsuc, Y.; Havkin-Frenkeld, D.; Dixona, R.A.; Ralph, J. A polymer of caffeyl alcohol in plant seeds. *Proc. Natl. Acad. Sci. USA* **2012**, *109*, 1772–1777. [CrossRef]
20. Fitzgerald, N.D. Chemistry challenges to enable a sustainable bioeconomy. *Nat. Rev. Chem.* **2017**, *1*, 0080. [CrossRef]
21. Strk, K.; Taccardi, N.; Bçsmann, A.; Wasserscheid, P. Oxidative Depolymerization of Lignin in Ionic Liquids. *ChemSusChem* **2010**, *3*, 719–723. [CrossRef]
22. de Wild, P.; Reith, H.; Heeres, E. Biomass pyrolysis for chemicals. *Biofuels* **2011**, *2*, 185–208. [CrossRef]
23. Holladay, J.E.; White, J.F.; Bozell, J.J.; Johnosn, D. *Top Value-Added Chemicals from Biomass. Volume II, Results of Screening for Potential Candidates from Biorefinery Lignin*; Prepared for the DOE, PNNL; Pacific Northwest National Lab: Richland, WA, USA, 2007; p. 16983.
24. Gosselink, R.J.A.; Teunissen, W.; van Dam, J.E.G.; de Jong, E.; Gellerstedt, G.; Scott, E.L.; Sanders, J.P.M. Lignin depolymerisation in supercritical carbon dioxide/acetone/water fluid for the production of aromatic chemicals. *Bioresour. Technol.* **2012**, *106*, 173–177. [CrossRef]
25. Hu, J.; Shen, D.; Wu, S.; Zhang, H.; Xiao, R. Composition Analysis of Organosolv Lignin and Its Catalytic Solvolysis in Supercritical Alcohol. *Energy Fuels* **2014**, *28*, 4260–4266. [CrossRef]
26. Chan, J.M.W.; Bauer, S.; Sorek, H.; Sreekumar, S.; Wang, K.; Toste, F.D. Studies on the Vanadium-Catalyzed Nonoxidative Depolymerization of Miscanthus giganteus-Derived Lignin. *ACS Catal.* **2013**, *3*, 1369–1377. [CrossRef]
27. Beckham, G.T.; Johnson, C.W.; Karp, E.M.; Salvachua, D.; Vardon, D.R. Opportunities and challenges in biological lignin valorization. *Curr. Opin. Biotechnol.* **2016**, *42*, 40–53. [CrossRef]
28. Wilkerson, C.G.; Mansfield, S.D.; Lu, F.; Withers, S.; Park, J.-Y.; Karlen, S.D.; Gonzales-Vigil, E.; Padmakshan, D.P.; Unda, F.; Rencoret, J.; et al. Monolignol Ferulate Transferase Introduces Chemically Labile Linkages into the Lignin Backbone. *Science* **2014**, *344*, 90–93. [CrossRef] [PubMed]
29. Li, Y.; Shuai, L.; Kim, H.; Motagamwala, A.M.; Mobley, J.K.; Yue, F.; Tobimatsu, Y.; Havkin-Frenkel, D.; Chen, F.; Dixon, R.A.; et al. An "ideal lignin" facilitates full biomass utilization. *Sci. Adv.* **2018**, *4*, eaau2968. [CrossRef]
30. Fuchs, G.; Boll, M.; Heider, J. Microbial degradation of aromatic compounds—From one strategy to four. *Nat. Rev. Microbiol.* **2011**, *9*, 803–816. [CrossRef] [PubMed]
31. Saa, L.; Jaureguibeitia, A.; Largo, E.; Llama, M.J.; Serra, J.L. Cloning, purification and characterization of two components of phenol hydroxylase from *Rhodococcus erythropolis* UPV-1. *Appl. Microbiol. Biotechnol.* **2010**, *86*, 201–211. [CrossRef] [PubMed]
32. Lingera, J.G.; Vardona, D.R.; Guarnieria, M.Y.; Karpa, E.M.; Hunsingera, G.B.; Frandena, M.A.; Johnson, C.W.; Chupkad, G.; Strathmannc, T.J.; Pienkosa, P.T.; et al. Lignin valorization through integrated biological funneling and chemical catalysis. *Proc. Natl. Acad. Sci. USA* **2014**, *111*, 12013–12018. [CrossRef]
33. Duan, J.; Huo, X.; Du, W.J.; Liang, J.D.; Wang, D.Q.; Yang, S.C. Biodegradation of kraft lignin by a newly isolated anaerobic bacterial strain, *Acetoanaerobium* sp. WJDL-Y2. *Lett. Appl. Microbiol.* **2015**, *62*, 55–62. [CrossRef]
34. Schink, B.; Müller, B.P.J. Anaerobic Degradation of Phenolic Compounds. *Naturwissenschaften* **2000**, *87*, 12–23. [CrossRef] [PubMed]
35. Carmona, M.; Zamarro, M.T.; Blazquez, B.; Durante-Rodríguez, G.; Juarez, J.F.; Valderrama, J.A.; Barragan, M.J.L.; García, J.L.; Eduardo Díaz, E. Anaerobic Catabolism of Aromatic Compounds: A Genetic and Genomic View. *Microbiol. Mol. Biol. Rev.* **2009**, *73*, 71–133. [CrossRef] [PubMed]
36. Tinikul, R.; Chenprakhon, P.; Maenpuen, S.; Chaiyen, P. Biotransformation of Plant-Derived Phenolic Acids. *Biotechnol. J.* **2018**, *13*, 1700632. [CrossRef] [PubMed]
37. Kourist, R.; Guterl, J.-K.; Miyamoto, K.; Sieber, V. Enzymatic Decarboxylation—An Emerging Reaction for Chemicals Production from Renewable Resources. *ChemCatChem* **2014**, *6*, 689–701. [CrossRef]
38. Aresta, M.; Dibenedetto, A. Enzymatic Conversion of CO_2 (Carboxylation Reactions and Reduction to Energy-Rich C1 Molecules). In *Reaction Mechanisms in Carbon Dioxide Conversion*; Aresta, M., Dibenedetto, A., Quaranta, E., Eds.; Springer: Berlin/Heidelberg, Germany, 2016; pp. 347–371.

39. Aresta, M.; Dibenedetto, A. Development of environmentally friendly syntheses: Use of enzymes and biomimetic systems for the direct carboxylation of organic substrates. *Rev. Mol. Biotechnol.* **2002**, *90*, 113–128. [CrossRef]
40. Lewin, R.; Thompson, M.L.; Micklefield, J. Enzyme Carboxylation and Decarboxylation. In *Science of Synthesis: Biocatalysis in Organic Synthesis*; Faber, K., Fessner, W.-D., Turner, N.J., Eds.; Thieme: Stuttgart, NY, USA, 2015; Volume 2, pp. 133–157.
41. Yoshida, T.; Nagasawa, T. Chapter 5—Biological Kolbe-Schmitt carboxylation: Possible use of enzymes for the direct carboxylation of organic substrates. In *Future Directions in Biocatalysis*; Elsevier: Amsterdam, The Netherlands, 2007; pp. 83–105.
42. Glueck, S.M.; Gümüs, S.; Fabian, W.M.F.; Faber, K. Biocatalytic carboxylation. *Chem. Soc. Rev.* **2010**, *39*, 313–328. [CrossRef]
43. Pesci, L.; Glueck, S.M.; Gurikov, P.; Smirnova, I.; Faber, K.; Liese, A. Biocatalytic carboxylation of phenol derivatives: Kinetics and thermodynamics of the biological Kolbe–Schmitt Synthesis. *FEBS J.* **2015**, *282*, 1334–1345. [CrossRef]
44. Silverman, R.B. *The Organic Chemistry of Enzyme-Catalyzed Reactions*; Chapter 7, Carboxylations; Academic Press: San Diego, CA, USA, 2002; pp. 289–320.
45. Wuensch, C.; Gross, J.; Steinkellner, G.; Lyskowski, A.; Gruber, K.; Glueck, S.M.; Faber, K. Regioselective ortho-carboxylation of phenols catalyzed by benzoic acid decarboxylases: A biocatalytic equivalent to the Kolbe–Schmitt reaction. *RSC Adv.* **2014**, *4*, 9673–9679. [CrossRef]
46. Erb, T.J. Carboxylases in natural and synthetic microbial pathways. *Appl. Environ. Microbiol.* **2011**, *77*, 8466–8477. [CrossRef]
47. Schmeling, S.; Fuchs, G. Anaerobic metabolism of phenol in proteobacteria and further studies of phenylphosphate carboxylase. *Arch. Microbiol.* **2009**, *191*, 869–878. [CrossRef]
48. Yoshida, M.; Fukuhara, N.; Oikawa, T. Thermophilic, reversible γ-resorcylate decarboxylase from *Rhizobium* sp. strain MTP-10005: Purification, molecular characterization, and expression. *J. Bacteriol.* **2004**, *186*, 6855–6863. [CrossRef] [PubMed]
49. Yoshida, M.; Oikawa, T.; Obata, H.; Abe, K.; Mihara, H.; Esaki, N. Biochemical and genetic analysis of the γ-resorcylate (2,6-dihydroxybenzoate) catabolic pathway in *Rhizobium* sp. strain MTP-10005: Identification and functional analysis of its gene cluster. *J. Bacteriol.* **2007**, *189*, 1573–1581. [CrossRef] [PubMed]
50. Ishii, Y.; Narimatsu, Y.; Iwasaki, Y.; Arai, N.; Kino, K.; Kirimura, K. Reversible and nonoxidative gamma-resorcylic acid decarboxylase: Characterization and gene cloning of a novel enzyme catalyzing carboxylation of resorcinol, 1,3-dihydroxybenzene, from *Rhizobium radiobacter*. *Biochem. Biophys. Res. Commun.* **2004**, *324*, 611–620. [CrossRef] [PubMed]
51. Yoshida, T.; Hayakawa, Y.; Matsui, T.; Nagasawa, T. Purification and characterization of 2,6-dihydroxybenzoate decarboxylase reversibly catalyzing nonoxidative decarboxylation. *Arch. Microbiol.* **2004**, *181*, 391–397. [CrossRef] [PubMed]
52. Matsui, T.; Yoshida, T.; Yoshimura, T.; Nagasawa, T. Regioselective carboxylation of 1,3-dihydroxybenzene by 2,6-dihydroxybenzoate decarboxylase of *Pandoraea* sp. 12B-2. *Appl. Microbiol. Biotechnol.* **2006**, *73*, 95–102. [CrossRef] [PubMed]
53. Kasai, D.; Araki, N.; Motoi, K.; Yoshikawa, S.; Iino, T.; Imai, S.; Masai, E.; Fukuda, M. γ-Resorcylate catabolic-pathway genes in the soil actinomycete *Rhodococcus jostii* RHA1. *Appl. Environ. Microbiol.* **2015**, *81*, 7656–7665. [CrossRef] [PubMed]
54. Sheng, X.; Patskovsky, Y.; Vladimirova, A.; Bonanno, J.B.; Almo, S.C.; Himo, F.; Frank, M.; Raushel, F.M. Mechanism and Structure of γ-Resorcylate Decarboxylase. *Biochemistry* **2018**, *57*, 3167–3175. [CrossRef]
55. Santa, R.; Rao, N.A.; Vaidyanathan, C.S. Identification of the active-site peptide of 2,3-dihydroxybenzoic acid decarboxylase from *Aspergillus oryzae*. *Biochim. Biophys. Acta* **1996**, *1293*, 191–200. [CrossRef]
56. NCBI Database, GemBank: EXM04459.1, 2,3-dihydroxybenzoate decarboxylase [*Fusarium oxysporum* f. sp. Cubense tropical race 4 54006]. 2015. Available online: https://www.ncbi.nlm.nih.gov/search/all/?term=EXM04459.1 (accessed on 28 December 2018).
57. Ywasaki, Y.; Gunji, H.; Kino, K.; Hottori, T.; Ishii, Y.; Kirimura, K. Novel metabolic pathway for salicylate biodegradation via phenol in yeast *Trichosporon moniliiforme*. *Biodegradation* **2010**, *21*, 557–564. [CrossRef]

58. Patskovsky, V.A.; Fedorov, Y.; Bonanno, A.A.; Fedorov, J.B.; Toro, E.V.; Hillerich, R.; Seidel, B.; Richards, N.R.D.; Almo, S.C.; Raushel, F.M. Substrate distortion and the catalytic reaction mechanism of 5-carboxyvanillate decarboxylase. *J. Am. Chem. Soc.* **2016**, *138*, 826–836.
59. Xiang, S.; Zhu, W.; Huddleston, J.; Xiang, D.F.; Raushel, F.M.; Richards, N.G.J.; Himo, F. A combined experimental-theoretical study of the ligW-catalyzed decarboxylation of 5-carboxyvanillate in the metabolic pathway for lignin degradation. *ACS Catal.* **2017**, *7*, 4968–4974.
60. Enzymatic carboxylation reactions are highly selective. Therefore often Authors report the amount of a specific compound undergoing the reaction as "% conversion". In this review we will adopt the terms "% conversion" and "% yield" as used by Authors in the original papers.
61. Plasch, K.; Resch, V.; Hitce, J.; Popłoński, J.; Faber, K.; Glueck, S.M. Regioselective Enzymatic Carboxylation of Bioactive (Poly) phenols. *Adv. Synth. Catal.* **2017**, *359*, 959–965. [CrossRef]
62. Quideau, S.; Deffieux, D.; Douat-Casassus, C.; Pouysgu, L. Plant Polyphenols: Chemical Properties, Biological, Activities, and Synthesis. *Angew. Chem. Int. Ed.* **2011**, *50*, 586–621. [CrossRef] [PubMed]
63. Klausing, K.; Smith, V.; Shen, M.-J.R.; Moore, J.; Hall, K. Methods Using Polyphenols for Inhibiting Light-Induced Degradation of Nucleic Acids and for Detecting Fluorescent-Tagged Nucleic Acids. U.S. Patent 20120196758A1, 2 August 2012.
64. Plasch, K.; Hofer, G.; Keller, W.; Hay, S.; Heyes, D.J.; Dennig, A.; Glueck, S.M.; Faber, K. Pressurized CO_2 as a carboxylating agent for the biocatalytic *ortho*-carboxylation of resorcinol. *Green Chem.* **2018**, *20*, 1754–1759. [CrossRef]
65. Ren, J.; Yao, P.; Yu, S.; Dong, W.; Chen, Q.; Feng, J.; Wu, Q.; Zhu, D. An Unprecedented Effective Enzymatic Carboxylation of Phenols. *ACS Catal.* **2016**, *6*, 564–567. [CrossRef]
66. Zhanga, X.; Renb, J.; Yaob, P.; Gong, R.; Wanga, M.; Wub, Q.; Zhu, D. Biochemical characterization and substrate profiling of a reversible 2,3-dihydroxybenzoic acid decarboxylase for biocatalytic Kolbe-Schmitt reaction. *Enzym. Microb. Technol.* **2018**, *113*, 37–43. [CrossRef] [PubMed]
67. Pesci, L.; Gurikov, P.; Liese, A.; Kara, S. Amine-Mediated Enzymatic Carboxylation of Phenols Using CO_2 as Substrate Increases Equilibrium Conversions and Reaction Rates. *Biotechnol. J.* **2017**, *12*, 1700332. [CrossRef]
68. Kirimura, K.; Gunji, H.; Wakayama, R.; Hattori, T.; Ishii, Y. Enzymatic Kolbe–Schmitt reaction to form salicylic acid from phenol: Enzymatic characterization and gene identification of a novel enzyme, Trichosporon moniliiforme salicylic acid decarboxylase. *Biochem. Biophys. Res. Commun.* **2010**, *394*, 279–284. [CrossRef]
69. Kirimura, K.; Yanaso, S.; Kosaka, S.; Koyama, K.; Hattori, T.; Ishii, Y. Production of *p*-Aminosalicylic Acid through Enzymatic Kolbe Schmitt Reaction Catalyzed by Reversible Salicylic Acid Decarboxylase. *Chem. Lett.* **2011**, *40*, 206–208. [CrossRef]
70. Ienaga, S.; Kosaka, S.; Honda, Y.; Ishii, Y.; Kirimura, K. p-Aminosalicylic Acid Production by Enzymatic Kolbe-Schmitt Reaction Using Salicylic Acid Decarboxylases Improved through Site-Directed Mutagenesis. *Bull. Chem. Soc. Jpn.* **2013**, *86*, 628–634. [CrossRef]
71. Peng, X.; Masai, E.; Kitayama, H.; Harada, K.; Katayama, Y.; Fukuda, M. Cloning and Characterization of the Ferulic Acid Catabolic Genes of *Sphingomonas paucimobilis* SYK-6. *Appl. Environ. Microb.* **2002**, *68*, 4416–4424.
72. Peng, X.; Masai, E.; Kasai, D.; Miyauchi, K.; Katayama, Y.; Fukuda, M. A Second 5-Carboxyvanillate Decarboxylase Gene, *ligW2* Is Important for Lignin-Related Biphenyl Catabolism in *Sphingomonas paucimobilis* SYK-6. *Appl. Environ. Microb.* **2005**, *71*, 5014–5021. [CrossRef] [PubMed]
73. Peng, C.; Liu, Y.; Guo, X.; Liu, W.; Li, Q.; Zhao, Z.K. Selective carboxylation of substituted phenols with engineered Escherichia coli whole-cells. *Tetrahedron Lett.* **2018**, *59*, 3810–3815. [CrossRef]
74. Goto, M.; Hayashi, H.; Miyahara, I.; Hirotsu, K.; Yoshida, M.; Oikawa, T. Crystal Structures of Non-oxidative Zinc-dependent 2,6-Dihydroxybenzoate (γ-Resorcylate) Decarboxylasefrom *Rhizobium* sp. Strain MTP-10005. *J. Biol. Chem.* **2006**, *281*, 34365–34373. [CrossRef] [PubMed]
75. Bordoli, L.; Kiefer, F.; Arnold, K.; Benkert, P.; Battey, J.; Schwede, T. Protein structure homology modeling using SWISS-MODEL workspace. *Nat. Protoc.* **2009**, *4*, 1–13. [CrossRef] [PubMed]
76. Pesci, L.; Kara, S.; Liese, A. Evaluation of the Substrate Scope of Benzoic Acid (De)carboxylases According to Chemical and Biochemical Parameters. *ChemBioChem* **2016**, *17*, 1845–1850. [CrossRef] [PubMed]
77. Matsui, T.; Yoshida, T.; Hayashi, T.; Nagasawa, T. Purification, characterization, and gene cloning of 4-hydroxybenzoate decarboxylase of Enterobacter cloacae P240. *Arch. Microbiol.* **2006**, *186*, 21–29. [CrossRef]
78. Liu, J.; Zhang, X.; Zhou, S.; Tao, P.; Liu, J. Purification and characterization of a 4-hydroxybenzoate decarboxylase from Chlamydophila pneumonia AR39. *Curr. Microbiol.* **2007**, *54*, 102–107. [CrossRef]

79. Li, T.; Juteau, P.; Beaudet, R.; Lepine, F.; Villemur, R.; Bisaillon, J-G. Purification and characterization of a 4-hydroxybenzoate decarboxylase from an anaerobic coculture. *Can. J. Microbiol.* **2000**, *46*, 856–859. [CrossRef]
80. Tschech, A.; Fuchs, G. Anaerobic degradation of phenol by pure cultures of newly isolated denitrifying pseudomonads. *Arch. Microbiol.* **1987**, *148*, 213–217. [CrossRef]
81. Lack, A.; Tommasi, I.; Aresta, M.; Fuchs, G. Catalytic properties of phenol carboxylase in vitro study of CO_2: 4-hydroxybenzoate isotope exchange reaction. *Eur. J. Biochem.* **1991**, *197*, 473–479. [CrossRef] [PubMed]
82. Xie, X.; Muller, N. Enzymes involved in the anaerobic degradation of phenol by the sulfate-reducing bacterium *Desulfatiglans anilini*. *BMC Microbiol.* **2018**, *18*, 93. [CrossRef] [PubMed]
83. Khanna, P.; Rajkumar, B.; Jothikumar, N. Anoxygenic degradation of aromatic substances by *Rhodopseudomonas palustris*. *Curr. Microbiol.* **1992**, *25*, 63–67. [CrossRef] [PubMed]
84. Yoshida, T.; Inami, Y.; Matsui, T.; Nagasawa, T. Regioselective carboxylation of catechol by 3,4-dihydroxybenzoate decarboxylase of Enterobacter cloacae P241. *Biotechnol. Lett.* **2010**, *32*, 701–705. [CrossRef] [PubMed]
85. He, Z.; Wiegel, J. Purification and characterization of an oxygensensitive, reversible 3,4-dihydroxybenzoate decarboxylase from *Clostridium hydroxybenzoicum*. *J Bacteriol.* **1996**, *178*, 3539–3543. [CrossRef] [PubMed]
86. Lupa, B.; Lyon, D.; Shaw, L.N.; Sieprawska-Lupa, M.; Wiegel, J. Properties of the reversible nonoxidative vanillate/4-hydroxybenzoate decarboxylase from *Bacillus subtilis*. *Can. J. Microbiol.* **2008**, *54*, 75–81. [CrossRef] [PubMed]
87. Wuensch, C.; Pavkov-Keller, T.; Steinkellner, G.; Gross, J.; Fuchs, M.; Hromic, A.; Lyskowski, A.; Fauland, K.; Gruber, K.; Glueck, S.M.; et al. Regioselective Enzymatic β-Carboxylation of para-Hydroxystyrene Derivatives Catalyzed by Phenolic Acid Decarboxylases. *Adv. Synth. Catal.* **2015**, *357*, 1909–1918. [CrossRef] [PubMed]
88. Wuensch, C.; Glueck, S.M.; Gross, J.; Koszelewski, D.; Schober, M.; Faber, K. Regioselective Enzymatic Carboxylation of Phenols and Hydroxystyrene Derivatives. *Org. Lett.* **2012**, *14*, 1974–1977. [CrossRef]
89. Gu, W.; Yang, J.; Lou, Z.; Liang, L.; Sun, Y.; Huang, J.; Li, X.; Cao, Y.; Meng, Z.; Zhang, K.-Q. Structural Basis of Enzymatic Activity for the Ferulic Acid Decarboxylase (FADase) from *Enterobacter* sp. Px6-4. *PLoS ONE* **2011**, *6*, e16262. [CrossRef]
90. Sheng, X.; Himo, K. Theoretical Study of Enzyme Promiscuity: Mechanisms of Hydration and Carboxylation Activities of Phenolic Acid Decarboxylase. *ACS Catal.* **2017**, *7*, 1733–1741. [CrossRef]
91. Aleku, G.A.; Prause, C.; Bradshaw-Allen, R.T.; Plasch, K.; Glueck, S.M.; Bailey, S.S.; Payne, K.A.P.; Parker, D.A.; Faber, K.; Leys, D. Terminal Alkenes from Acrylic Acid Derivatives via Non-Oxidative Enzymatic Decarboxylation by Ferulic Acid Decarboxylases. *ChemCatChem* **2018**, *10*, 1–11. [CrossRef] [PubMed]
92. Meckenstock, R.U.; Boll, M.; Mouttaki, H.; Koelschbach, J.S.; Cunha Tarouco, P.; Weyrauch, P.; Don, X.; Himmelberg, A.M. Anaerobic Degradation of Benzene and Polycyclic Aromatic Hydrocarbons. *J. Mol. Microbiol. Biotechnol.* **2016**, *26*, 92–118. [CrossRef] [PubMed]
93. Atashgahi, S.; Hornung, B.; van der Waals, M.J.; Nunes da Rocha, U.; Hugenholtz, F.; Nijsse, B.; Molenaar, D.; van Spanning, R.; Stams, A.J.M.; Gerritse, J.; et al. A benzene-degrading nitrate reducing microbial consortium displays aerobic and anaerobic benzene degradation pathways. *Sci. Rep.* **2018**, *8*, 4490. [CrossRef] [PubMed]
94. Laban, N.A.; Selesi, D.; Rattei, T.; Tischler, P.; Meckenstock, R.U. Identification of enzymes involved in anaerobic benzene degradation by a strictly anaerobic iron-reducing enrichment culture. *Environ. Microbiol.* **2010**, *12*, 2783–2796. [CrossRef] [PubMed]
95. Mouttaki, H.; Johannes, J.; Meckenstock, R.U. Identification of naphthalene carboxylase as a prototype for the anaerobic activation of non-substituted aromatic hydrocarbons. *Environ. Microbiol.* **2012**, *14*, 2770–2774. [CrossRef] [PubMed]
96. Oulame, M.Z.; Pion, F.; Allauddin, S.; Raju, K.V.S.N.; Ducrot, P.-H.; Allais, F. Renewable alternating aliphatic-aromatic poly(ester-urethane)s prepared from ferulic acid and bio-based diols. *Eur. Polym. J.* **2015**, *63*, 186–193. [CrossRef]
97. Sun, Z.; Bottari, G.; Afanasenko, A.; Stuart, M.C.A.; Deuss, P.J.; Fridrich, B.; Barta, K. Complete lignocellulose conversion with integrated catalyst recycling yielding valuable aromatics and fuels. *Nat. Catal.* **2018**, *1*, 82–92. [CrossRef]

98. Barta, K.; Ford, P.C. Catalytic Conversion of Nonfood Woody Biomass Solids to Organic Liquids. *Acc. Chem. Res.* **2014**, *47*, 1503–1512. [CrossRef] [PubMed]
99. Ata, M.S.; Liu, Y.; Zhitomirsky, I. A review of new methods of surface chemical modification, dispersion and electrophoretic deposition of metal oxide particles. *RSC Adv.* **2014**, *4*, 22716–22732. [CrossRef]
100. Sedó, J.; Saiz-Poseu, J.; Busqué, F.; Ruiz-Molina, D. Catechol-Based Biomimetic Functional Materials. *Adv. Mater.* **2013**, *25*, 653–701. [CrossRef] [PubMed]
101. Wua, W.; Liua, F.; Singha, S. Toward engineering *E. coli* with an autoregulatory system for lignin valorization. *Proc. Natl. Acad. Sci. USA* **2018**, *115*, 2970–2975. [CrossRef] [PubMed]



© 2019 by the author. Licensee MDPI, Basel, Switzerland. This article is an open access article distributed under the terms and conditions of the Creative Commons Attribution (CC BY) license (http://creativecommons.org/licenses/by/4.0/).